Single cell transcriptomic comparison between mouse embryonic pancreas and pancreatic organoids generated from mouse embryonic stem cell-derived mesoderm and pancreatic progenitors

Shlomit Edri[1*], Vardit Rosenthal[1#], Or Ginsburg[1#], Abigail Newman Frisch[1], Christophe E. Pierreux[2], Nadav Sharon[3] and Shulamit Levenberg[1*]

[1]Faculty of Biomedical Engineering, Technion – Israel Institute of Technology, Haifa, Israel
[2]Cell Biology Unit, de Duve Institute, UCLouvain, Woluwe, Belgium
[3]Faculty of Biology, Technion – Israel Institute of Technology, Haifa, Israel

[#]Equal contribution.
*Corresponding authors: Shlomit Edri: shlomitedri@campus.technion.ac.il and Shulamit Levenberg: shulamit@bm.technion.ac.il

Author Contributions

Conceptualization: S.E. and S.L.; Methodology: S.E, N.S. and S.L.; Software: S.E.; Validation: S.E., V.R., O.G. and A.N.F.; Investigation: S.E., V.R. and O.G.; Resources: S.L.; Writing - original draft: S.E. and S.L.; Writing - review & editing: S.E., A.N.F., N.S., C.E.P. and S.L.; Supervision: S.L.; Funding acquisition: S.L. and C.E.P.

Abstract

In the mammalian embryo, the developing pancreas is surrounded by mesoderm compartments, which are important for generating the signals and mechanical constraints that induce the formation of the pancreatic bud and its differentiation. Most protocols of pancreatic organoid generation do not include this mesoderm niche and have partial success in capturing the full repertoire of the pancreas. This work aims to generate a pancreatic organoid by differentiating mouse embryonic stem cells (mESCs) under controlled conditions to mesoderm in parallel to pancreas identity, without the use of poorly defined extracellular matrix such as Matrigel. The first step in our work focused on mESCs differentiation in adherent culture. We were able to obtain a higher differentiation efficacy to definitive endoderm and specifically to pancreas progenitors (PPs) by first differentiating mESCs to epiblast stem cells (EpiSCs), a primed pluripotent state. Next, we built a three-dimension (3D) culture, by aggregating PPs with EpiSC-derived mesoderm progenitors (MPs), recapitulating cellular interactions occurring during embryonic pancreas development. Culture of these MP-PP organoids, referred here as pancreatic organoids, generated the different pancreatic cell types, i.e. endocrine, acinar and ductal cells, as well as blood vessel-like networks. Furthermore, single-cell RNA sequencing analysis of the pancreatic organoids revealed gene expression patterns similar to those of the mouse embryonic pancreas at E12, E14 and E17, primarily in the endocrine differentiation lineage.

Introduction

The pancreas is a gland with two main compartments, exocrine and endocrine, essential for digestion and glucose homeostasis, respectively. The endocrine function is achieved through the release of glucagon and insulin, two major hormones produced by alpha and beta cells respectively, which are required to maintain normal blood glucose levels. The exocrine compartment is composed of acinar cells, which synthesize, store and secrete enzymes, such as trypsin, amylase and lipase that break down proteins, carbohydrates and fats. These digestive enzymes are drained into the duodenum via a highly branched network of ducts running within the pancreas (Balak et al., 2019; Villasenor et al., 2010).

In early stage of development, mammalian embryos undergo gastrulation in which a single layered hollow sphere of cells reorganizes into a multi-layered structure. The primary function of gastrulation is to generate an axial system, to correctly position the germ layers in relation to one another for subsequent morphogenesis and to generate the mesoderm (Tam and Behringer, 1997) (Fig. S1A). In mammalian embryos, the pancreas develops from the endoderm, specifically from the gut tube endoderm in a region with proximity to the notochord, paired dorsal aortas artery and ventral vitelline veins which all derive from the mesoderm (Fig. S1B). The mesoderm-derived cells (Fig. S1A-B) are important for generating the signals and mechanical constraints that induce the formation of the pancreatic bud and its differentiation (Ghezelayagh et al., 2021; Ranjan et al., 2009).

Pluripotent stem cells (PSCs) are a good model to study pancreas organogenesis, since they recapitulate the dynamic expression of key genes involved in this developmental process. Figure S1C summarizes the course of the PSC in vitro differentiation, including the key genes expressed in each state (Byrnes et al., 2018; Jennings et al., 2015; Prabakar et al., 2012; Shih et al., 2013). PSCs are first differentiated to definitive endoderm (DE), which gives rise to many of the body's internal organs. After several differentiation states, DE finally differentiate into multipotent pancreatic progenitors (PPs) coexpressing Pdx1 and Nkx6-1. PPs are able to generate the various pancreatic cell types by further differentiating into acinar, duct and endocrine progenitors (Hohwieler et al., 2017; Nostro et al., 2015; Schaffer et al., 2010).

The last decade, pancreatic organoids have drawn the attention of researchers due to their powerful potential in studying pancreas development, disease modelling, drug testing and cellular therapy. Organoids are 3D in vitro models of stem cells or organ-specific progenitors that have the capacity to self-organize into specific structures that display architectures and functionalities similar to in vivo tissues and organs (Rossi et al., 2018). In addition to these interesting and promising similarities, organoids can be generated in large numbers, thereby offering the possibility to a diversity of manipulation.

Several protocols have been developed for the generation of pancreatic organoids from human pluripotent stem cell (PSC) ((Hohwieler et al., 2017; Kim et al., 2016; Koike et al., 2019; Nair et al., 2019) and reviewed in (Funata et al., 2020)). Although, mouse pancreatic organoids have also been generated from cells isolated from either adult pancreatic tissue or embryonic pancreas (Azzarelli et al., 2018; Greggio et al., 2013; Huch et al., 2013), the use of mouse PSC-based models are less common. During the organoid fabrication process, single cells or cell clusters are embedded in Matrigel, which provides mechanical support and serves as an extracellular matrix (ECM) substitute (Azzarelli et al., 2018; Greggio et al., 2013; Huch et al., 2013). However, the composition of Matrigel, mouse tumour-derived basement membrane ECM, suffers from batch-to-batch variability, thus rendering it is suboptimal for reproducible and complete studies focusing on cell self-organization process and signals during organogenesis.

Pancreatic organoids, either PSC-derived or tissue-derived organoids are limited in recapitulating the full tissue differentiation and do not reconstruct the mesoderm niche surrounding the developing pancreas. These pancreatic organoids usually lack specialized cell types, such as endothelial and mesenchymal support cells. Accordingly, in this work we decided to assemble a reproducible well-defined pancreatic organoid system that recapitulates pancreas development with its microenvironment, required for cell differentiation. Furthermore, we wanted that the new in vitro model will be comparable to its in vivo counterpart, the embryonic pancreas. To reach these goals our focus was on three aspects: 1) we used

mouse embryonic stem cells (mESCs) and interrogated the initial pluripotency state of the cells prior differentiation to achieve optimal pancreatic differentiation, 2) integrated mesoderm in the culture to develop a pancreatic niche, 3) avoided Matrigel usage to get better reproducibility. Our work investigated the potential of advancing mESCs to epiblast stem cells (EpiSCs), then to differentiate them and form a tissue-like environment in which EpiSC-derived PPs are in contact with EpiSC-derived mesoderm progenitors (MPs). Focusing on the mouse model enabled us to compare single-cell RNA-sequencing (scRNA-seq) of the mouse EpiSC-derived pancreatic organoids with mouse embryo pancreas at various embryonic stages, which revealed the presence of various pancreatic lineages.

Results

In vitro differentiation of EpiSCs to PPs passes through a rich definitive endoderm stage and results in high cell yield

Differentiation of mESCs usually starts when the cells are grown in the presence of either serum and leukemia inhibitory factor (LIF) (Moreau et al., 1988; Smith et al., 1988; Williams et al., 1988) or 2i, a cocktail of two inhibitors of ERK and GSK3 (Mulas et al., 2019; Wray et al., 2010; Ying et al., 2008). mESCs cultured in serum and LIF (referred to as SL) or in 2i are referred to as cells in a naïve or naïve ground state respectively. Specifically, it has been shown that differentiation to pancreatic lineages started when mESCs were in a naïve state (Borowiak et al., 2009; Delaspre et al., 2013). The majority of works on differentiating PSC to pancreas lineage showed advances in differentiating human PSCs towards pancreatic cell types (Borowiak et al., 2009; Chen et al., 2009; Hohwieler et al., 2017; Mamidi et al., 2018). It is known that human embryonic stem cells (ESCs) or human induced PSCs (iPSCs) are more similar to mouse epiblast stem cells, primed PSCs, rather than to ESCs at naïve or ground states (Edri et al., 2019a, 2019b; Fonseca et al., 2015; Morgani et al., 2017) (Fig. 1A). All the above led us to postulate and test whether advancing mESCs to EpiSCs can improve the efficacy of their differentiation to pancreatic progenitors, relaying on the field advances in human PSCs differentiation. Accordingly, we examined the response of mESCs in different states of pluripotency to pancreatic differentiation cues (Fig. 1A and Methods). Mouse ESCs in naïve and in ground states and EpiSCs were subjected to a 14 days differentiation protocol based on a human ESCs to PPs protocol (Hohwieler et al., 2017). At baseline, cells in the three starting conditions shared the expression of the core pluripotency factors Oct4, Nanog and Sox2 (Fig. 1B). Cells grown in 2i and SL expressed higher levels of Nanog and Sox2 in comparison to EpiSCs, which also expressed the epiblast-specific gene Fgf5 that was absent in mESCs (Fig. 1B and (Tosolini and Jouneau, 2015)).

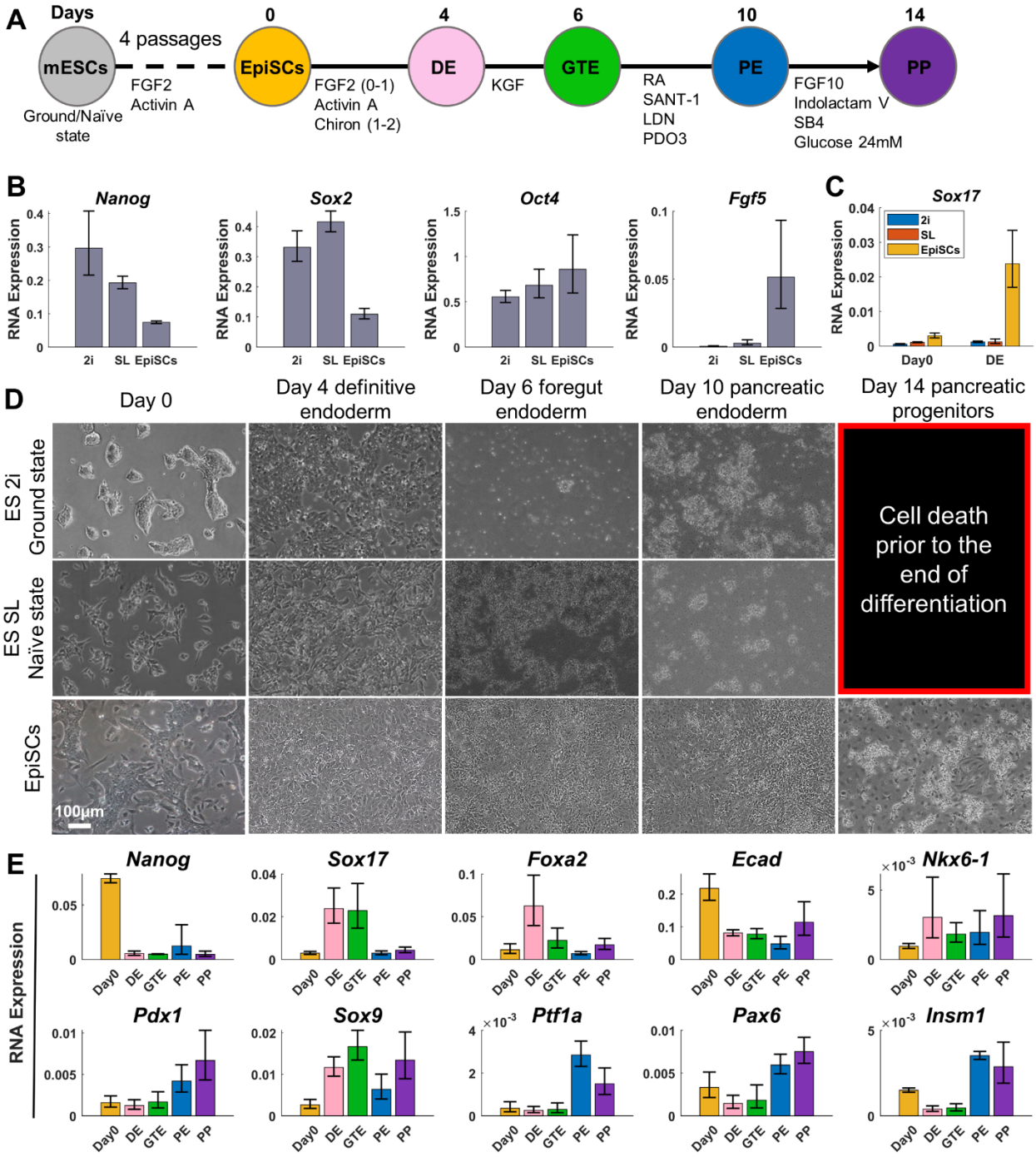

Figure 1. EpiSCs are a better source than ESCs for PP differentiation. A. In vitro differentiation course of mouse PSCs (modified from (Hohwieler et al., 2017)). The differentiation started either from mESCs at ground state (ES 2i), naïve (ES SL) or EpiSCs. **B.** Relative RNA expression obtained by RT-qPCR of the three pluripotency states prior differentiation. Cells expressed the pluripotency markers Nanog, Sox2 and Oct4. **C.** Sox17 expression obtained by RT-qPCR of the three differentiation conditions (different initial pluripotency states) at day 0 and DE stage. **D.** Cell morphology along the course of differentiation. **E.** Relative RNA expression obtained by RT-qPCR of pluripotency, endoderm and pancreatic gene markers during EpiSC differentiation to PPs. Data are presented as mean±SEM, n=3 biological experiments. mESCs, mouse embryonic stem cells; EpiSCs, epiblast stem cells; DE, definitive endoderm; GTE, gut tube endoderm; PE, pancreatic endoderm; PP, pancreatic progenitor.

ESCs starting their differentiation in 2i and SL growth medium, exhibited significant lower expression of Sox17 at differentiation day 4 (DE stage), in comparison to ESCs which were first transitioned to EpiSCs (Fig. 1C). Furthermore, ESCs starting their differentiation in 2i and SL growth medium, underwent cell death at around differentiation day 6. In contrast, when the differentiation began after transitioning ESCs to EpiSCs, cells survived longer and a high cell yield was obtained at the end of the differentiation period (Fig. 1D). We concluded that EpiSCs are superior to naïve ESCs for endoderm and specifically pancreas differentiation, which led us to carry on with investigating EpiSC differentiation to PPs.

Along the course of EpiSCs differentiation, mRNA expression (Methods and Fig. 1E) of the pluripotent markers Nanog and Ecad decreased, whilst the endodermal markers Sox17 and Foxa2 reached their highest levels at the DE and GTE stages (days 4 and 6, respectively). As the differentiation continued, Ecad expression remained constant between DE and PPs and there was a rise in the expression of pancreatic markers (Pdx1, Nkx6-1, Sox9, Ptf1a, Pax6, Insm1), mostly at PE and PP stages (days 10 and 14, respectively). Exploring the differentiation gene profile at the protein level (Methods, Fig. 2 and Fig. S2) identified an elevation of pancreatic markers and a reduction of Sox17 (endoderm) and of non-pancreas endoderm lineage markers (liver, lung, stomach and intestine, see Fig. S2) at the end of differentiation. Moreover, on differentiation day 14, most of the cells coexpressed SOX9/PDX1 and 89% of the cells coexpressed PDX1 and NKX6-1, indicating a highly efficient PP differentiation protocol (Fig. 2C).

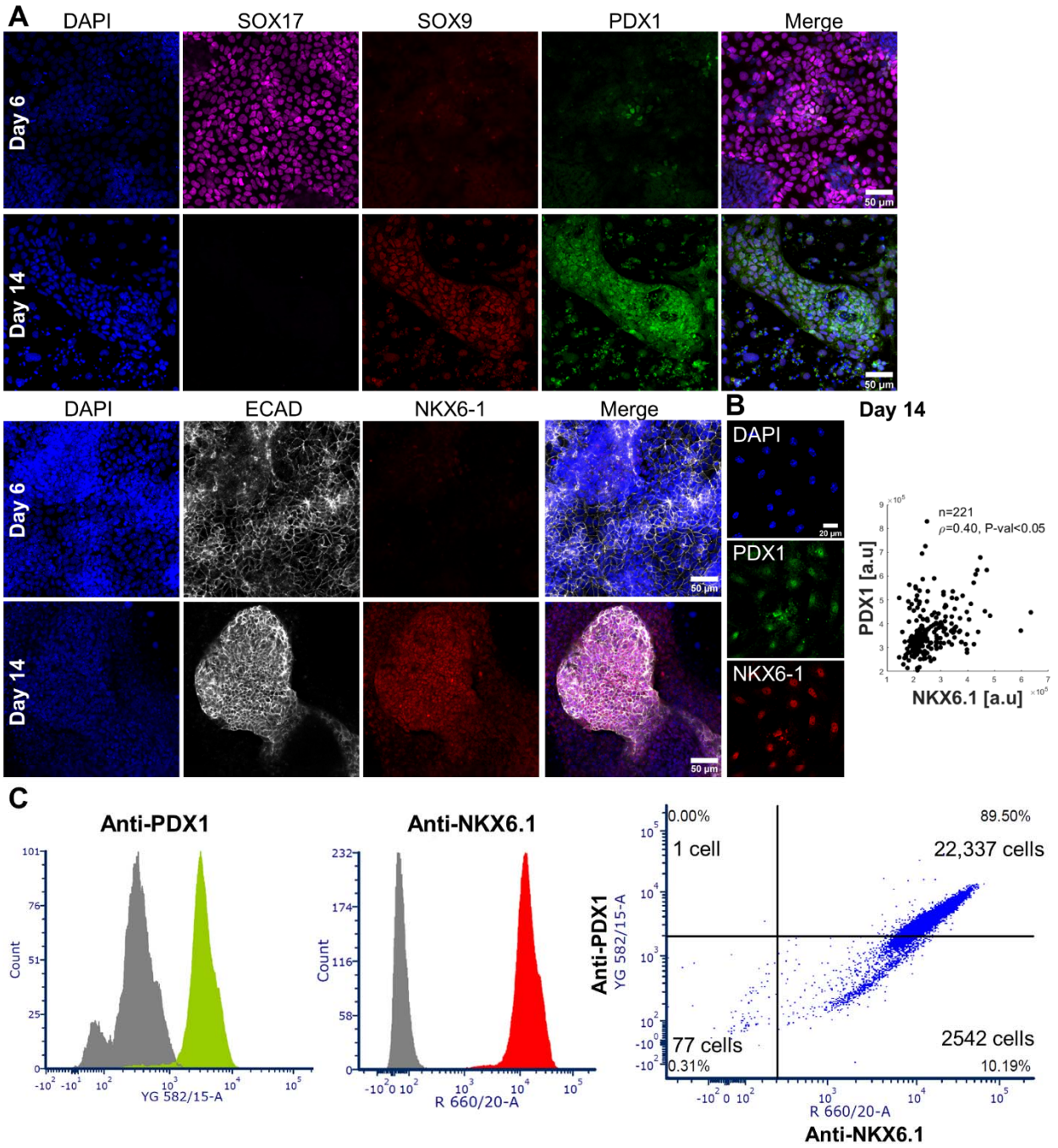

Figure 2. Pancreatic progenitors derived from epiblast stem cells. A. Confocal images captured along the course of EpiSC differentiation (day 6, the gut tube endoderm stage and day 14, pancreatic progenitor stage at the end of the differentiation). The cells were immunofluorescently stained for endoderm marker SOX17, pancreatic markers SOX9, NKX6-1 and epithelial marker ECAD. Note that SOX17 expression decreased from day 6 to day 14, whereas pancreatic marker expression increased. **B.** Higher magnification of confocal images immunofluorescently stained for PDX1 and NKX6-1 and nucleus intensity quantification. The number of cells analysed is denoted by n and ρ represents spearman's rank coefficient with P-value <0.05. **C.** Flow cytometry quantification of PDX1/NKX6-1 double-positive cells on day 14 of EpiSC differentiation to PPs.

3D pancreatic organoids exhibit epithelial, acinar, endocrine and endothelial markers

When grown alone, PP aggregates did not expanded over time (Fig. S5). We hypothesized that some inductive cues from another germ layer, most probably the mesoderm, was missing. To test this hypothesis, we used EpiSC-derived mouse caudle epiblast (CE) which has the characteristics of different type of mesoderm, including allantois cells and cells resembling the notochord (Edri et al., 2019a, 2019b). In the present work, we investigated whether this CE population can act as the in vitro mesoderm cells surrounding the PPs, recapitulating the developing pancreas and its niche in the embryo. Caudle epiblast cells, referred to here as MPs, were mixed with PPs in a ratio that corresponds to that observed in the mouse embryo pancreas (Glorieux et al., 2022). Each well of a 96-well plate was seeded with 1000 cell mixture (Fig 3A), and cells aggregated rapidly to form a round structure within 3 days. Culture continued for another 4 days on an orbital shaker (Fig 3B).

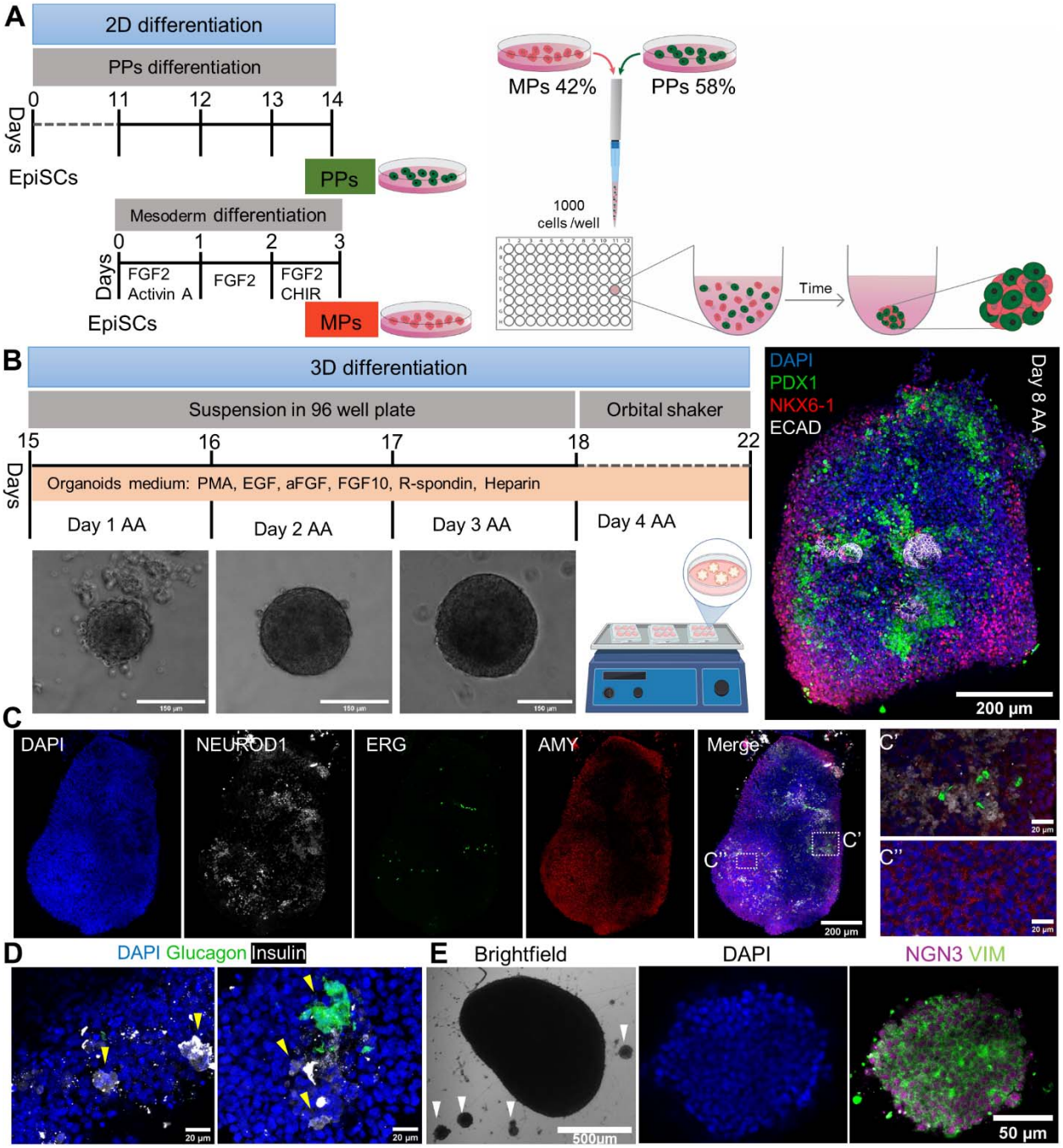

Figure 3. 3D culture of pancreatic progenitors with mesoderm progenitors recapitulates the developing pancreas in the embryo. A-B. A schematic illustration of a pancreatic organoid preparation. Prior to PP and MP aggregation, 2D differentiation courses of 14 days and 3 days were carried out to obtain PPs and MPs, respectively. **A.** On day 14, PPs and MPs were mixed at a proportion of 58% and 42% and 1000 mixed cells were plated in each well of a U-bottom 96 well plate. **B.** Brightfield images of the organoid on days 1, 2 and 3 after aggregation (AA). On day 4 AA, the aggregates were moved to a 6-well plate and placed on an orbital shaker for an additional 4 days. Confocal image of the organoid on day 8 AA immunofluorescently stained for ECAD, NKX6-1 and PDX1 (for higher magnification images see Fig. S3). **C-D.** Confocal images of organoids on day 8 AA immunofluorescently stained for endocrine marker NEUROD1, acinar marker AMY (Amylase), endothelial marker ERG (C, C', C''), and glucagon and insulin, which mark alpha and beta cells, respectively (D). Nuclear staining with DAPI is in blue. Yellow arrows in D

indicate regions of cells expressing insulin or glucagon. **E.** Brightfield image of the pancreatic organoid on day 8 after aggregation. The white arrows in the image show small aggregates that are approximately 100-150 µm in diameter, located around the organoid. A representative confocal image of a small aggregate immunofluorescently stained for vimentin (Vim), NGN3 and nuclei (DAPI).

Co-culture of PPs with MPs resulted in pancreatic organoids expressing the different pancreatic cell type genes along with mesenchymal and endothelial genes. On day 8 after aggregation (AA) the organoids expressed the pancreatic markers PDX1 and NKX6-1, contained epithelial regions marked by ECAD (Fig. 3B), endocrine cells expressing NEUROD1 and NGN3 (Neurog3), regions of acinar cells exhibiting AMY (amylase) expression, duct cells expressing SOX9 and weak expression of PDX1 and endothelial cells marked by ERG and CD31 expression (Fig S1C and Fig. 3 and Fig. S3-S4). Furthermore, in few regions in the PP-MP organoids, endocrine cells had differentiated into beta and alpha cells expressing insulin and glucagon, respectively (Fig. 3D, Fig. S4C).

Spatial proximity was noted between cells expressing the endothelial marker ERG and cells expressing the endocrine marker NEUROD1 (Fig. S4). Specifically, cells in the outer region of the organoid expressed AMY, whilst cells deeper in the tissue expressed less AMY and more NEUROD1 and ERG. This alignment between endothelial and endocrine cells (CD31 and NEUROD1 in Fig. S3, ERG and NEUROD1 in Fig. S4) mimics the preferential endothelial-endocrine cell organization found in the pancreas. Previous studies demonstrated the importance of endothelium for pancreas morphogenesis, differentiation and for induction endocrine differentiation in the embryo (Konstantinova and Lammert, 2004; Lammert et al., 2001, 2003; Pierreux et al., 2010; Ranjan et al., 2009)

During organoid culture, cells at and around the aggregate boundary had an elongated morphology, and formed several small 50-100um aggregates, suggesting that the cells are mesenchymal with migratory characteristics (Fig. 3E). Immunostaining of the small aggregates showed that most of the cells expressed the epithelial-mesenchymal transition (EMT) marker vimentin (Vim) and the transient endocrine marker NGN3 (Fig. 3E), similar to the profile of differentiating endocrine progenitors in the embryo (Gouzi et al., 2011; Larsen and Grapin-Botton, 2017; Pan and Wright, 2011; Rukstalis and Habener, 2007; Sharon et al., 2019a).

Single-cell RNA sequencing analysis revealed mainly mesenchymal and endocrine identities of the pancreatic organoids

To get the global picture of the pancreatic organoids and reveal the various cell populations they contain, we subjected the organoids to single-cell RNA-sequencing (scRNA-seq).

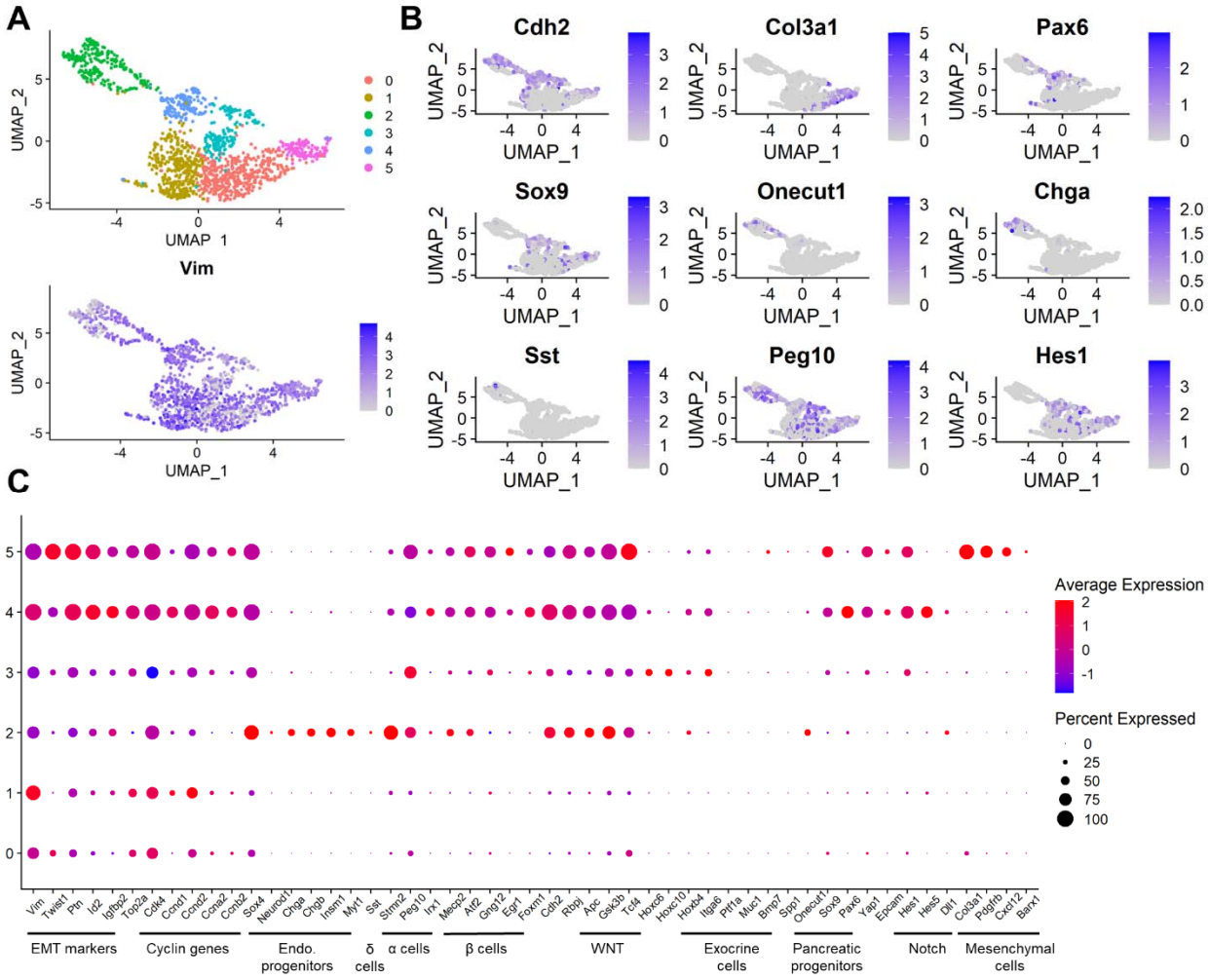

Figure 4. Pancreatic organoids show mesenchymal identity and endocrine populations. A. Upper graph shows dimensionality reduction UMAP plot of pancreatic organoids (1475 cells) grouped using the Seurat graph-based clustering method (Hao et al., 2021). The clustering algorithm (Methods) identified 6 clusters. At the bottom, Vim expression projected on the UMAP plot. **B.** Gene expression of selected genes projected on the UMAP plot. Colour intensity indicates level of expression. **C.** Expression dot plot of selected genes grouped by signalling pathway and cell identity categories (see Table S1). The size of the dot corresponds to the percentage of cells expressing a gene in each cluster. The colour represents the average expression level. UMAP, uniform manifold approximation and projection. Endo. progenitors, endocrine progenitors.

After filtering (see Methods), scRNA-seq of the pancreatic organoid resulted in a total of 1475 cells. Using a graph-based clustering algorithm (R package Seurat v4.0) we revealed 6 clusters, which were visualized using Uniform Manifold Approximation and Projection (UMAP) dimensionality reduction technique (Fig. 4A-B). Looking at our genes of interest (Fig. 4C) and marker genes of each cluster (Fig.S6), revealed clusters with EMT markers (all clusters and predominantly in cluster 0 and 1), cyclin genes (cluster 1), regulation of microtubule genes (cluster 2), hox genes (cluster 3), retinoic acid and pax genes (cluster 2 and 4), and mesenchymal genes (cluster 5). Most of the cells expressed Vim (Fig. 4A), suggesting migratory and motility capacities. Many cells, specifically in clusters 2, 3 and 4, expressed Cdh2, also known as N-cadherin. A study that explored the expression of N-cadherin in normal human tissues suggested that N-cadherin expression is closely associated with hormone-producing cells in the

pancreas but is not expressed in exocrine cells (Tsuchiya et al., 2006). Cluster 4 contained a cell population exhibiting a progenitor signature (Onecut1, Pax6, Sox9), cluster 2 predominantly held endocrine progenitors (Sox4, Chga, Chgb, Neurod1) and clusters 2-5 included various endocrine cell types (alpha, beta and delta cells). Although some cells exhibiting expression of genes found in alpha and beta cells (Fig. 4C and Table S1) were identified, expression of insulin (Ins1, beta cells) and glucagon (Gcg, alpha cells) was not detected in the scRNA-seq dataset. Only somatostatin (Sst, see Table S1), which is secreted by pancreatic delta cells, was detected in our dataset. Several cells across the clusters expressed exocrine progenitor markers (Ptf1a, Bmp7) and ductal markers (Muc1, Itga6). Nevertheless most of the clusters exhibited expression of EMT markers, with populations that had a dominant endocrine and mesenchyme identity, associated with cyclin genes like in the embryo ((Byrnes et al., 2018; Georgia et al.; Kim and Rane, 2011; Kushner et al., 2005) and Table S1).

The incomplete endocrine differentiation led us to investigate the pathways related to the endocrine lineage. We investigated the expression of genes related to Notch and Wnt signaling pathways, as well as Yap1, which is part of the hippo signaling pathway. These pathways play a significant role in determining endocrine versus ductal cell lineage (McCracken and Wells, 2012; Wu et al., 2021). Cluster 2 had low expression of Notch markers and high expression of Wnt markers, suggesting its endocrine identity.

The Hox gene expression reflect spatiotemporal information of the emerging embryonic axial tissues ((Young et al., 2009) and reviewed in (Deschamps and Duboule, 2017)). Exploring their expression in the organoid might help anchor it to a developmental stage and region in relation to the embryo. Hoxb4 was mainly expressed in clusters 3 and 4, whereas Hoxc6 and Hoxc10 were mainly expressed in cluster 3, suggesting that cluster 3 defines a more advanced developmental stage and more posterior embryonic region as compared to cluster 4. Furthermore, Hoxb4 takes part in limiting the endoderm response to signals from the notochord during the formation of the dorsal pancreatic bud (Kuo et al., 2019), this early stage of the pancreas might correlate with the progenitor population residing in cluster 4. Hoxc6 is expressed exclusively in the mesoderm of the developing pancreas and is needed for endocrine cell differentiation (Kuo et al., 2019; Larsen et al., 2015), suggesting a mesodermal state for cluster 3.

The pancreatic organoid captured many pancreatic cell types of the mouse embryonic pancreas

To further characterize the co-culture system and evaluate its limitations, we compared scRNA-seq data obtained from our pancreatic organoids and from mouse embryo pancreases at E12, E14 and E17 ((Byrnes et al., 2018) and see Methods).

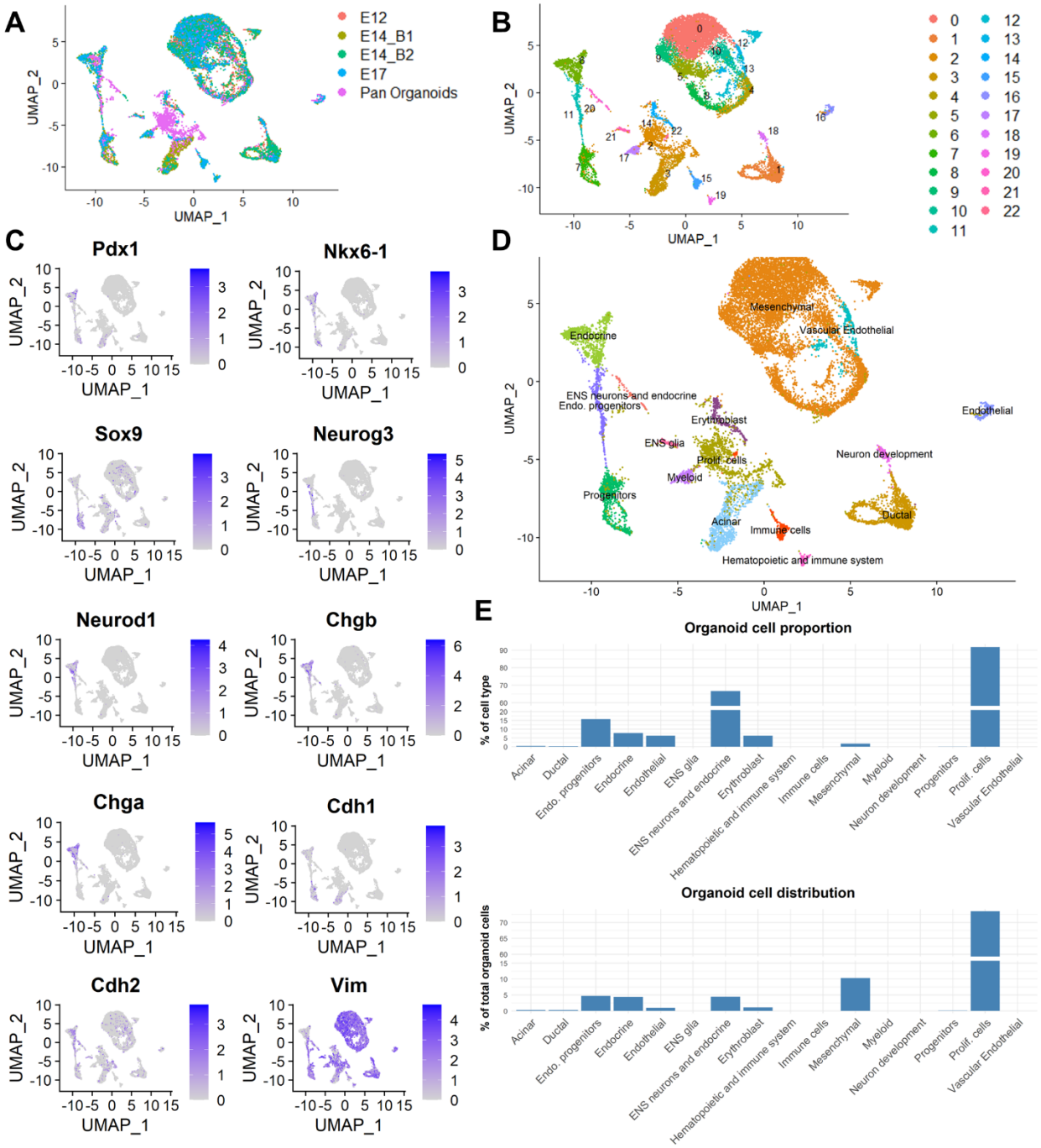

Figure 5. Comparison of single-cell RNA-seq of pancreatic organoids and mouse embryo pancreases reveals cell population overlap. A. UMAP visualization of single-cell RNA sequencing of pancreatic organoids (1475 cells) and of the mouse embryonic pancreas at E12 (4412 cells), 2 batches at E14: E14_B1 (3495 cells), E14_B2 (4309 cells) and E17 (2241 cells). Datasets were integrated using the Seurat integration algorithm (Hao et al., 2021) **B.** Seurat graph-based clustering revealed 23 clusters. **C.** Gene expression of selected genes projected on the UMAP plot. Colour intensity indicates level of expression. **D.** A UMAP plot showing the assignment of cell type to clusters. Clusters were identified based on the expression of known markers of different pancreatic cell types as in C and detailed in Table S2. **E.** Upper graph shows the percentage of the organoid cells in each cell type group and the

bottom graph shows the distribution of the organoid cells amongst the different cell type groups. Prolif. cells, proliferating cells; Endo. progenitors, endocrine progenitors; ENS, enteric nervous system.

Integration of the organoid and embryonic datasets yielded a UMAP with 23 cell clusters (Fig. 5A-B). Most interestingly, Key gene expression patterns (Fig. 5C) reflected a transition from a progenitor (cluster 7: Pdx1, Sox9 and Nkx6-1) to an endocrine progenitor population (cluster 11: Neurog3), which was later committed to endocrine lineage (cluster 6: Chga, Chgb and Neurod1). Interestingly, high levels of Vim expression was recorded in all cell populations, excluding the endocrine population, consistent with the observation that Vim is lost just after the hormones are turned on during endocrine differentiation (Sharon et al., 2019a). Exploring the gene marker profiles of each cluster (Methods and Table S2) allowed us to decipher the cell identity of each cluster, which is summarized on the UMAP plot in Figure 5D. We could not assign a clear pancreatic identity to Cluster 2 but did identify genes that were related to differentiating stem cells and amplifying cells, hence we called this cluster Proliferating cells (Prolif. cells).

The organoids were composed of various cell types that were found in the embryonic samples, mainly mesenchymal and endocrine cells, together with some exocrine, erythroblast and enteric nervous system (ENS) neurons (Fig. 5E). Approximately, 72% of the organoid cells were from cluster 2 (Prolif. cells) and 90% of cluster 2 was composed of organoid cells (Fig. 5E). In parallel, 0.95% of the organoid cells were endothelial, matching the proportions in the embryo at E14 (batch 1 with 0.92% and batch 2 with 1.04%, Table S4).

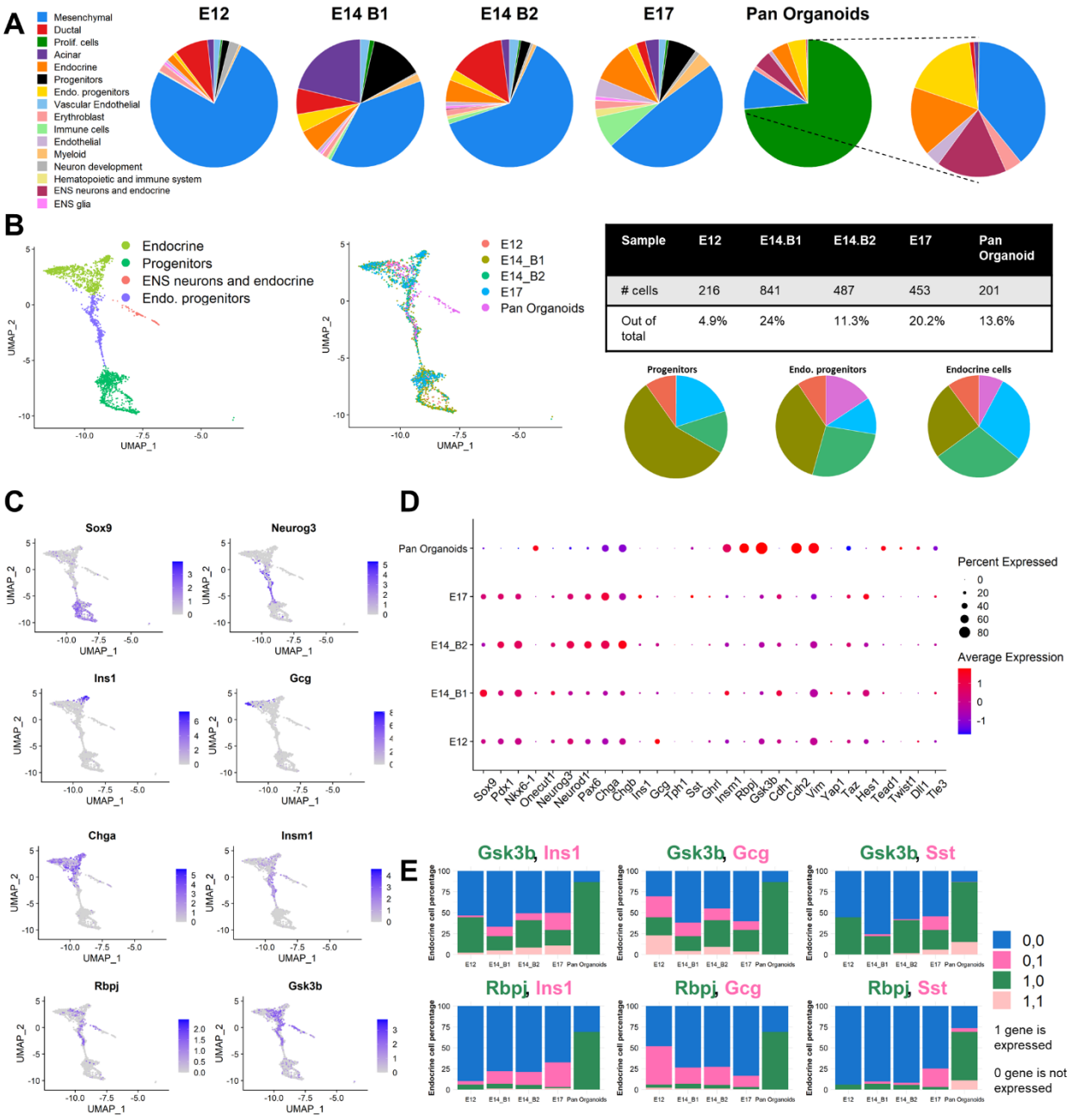

Figure 6. Most of the organoid-embryo similarity is in the endocrine compartment. A. Pie plots showing the proportion of the different cell types in the mouse embryo at E12, E14 and E17 and the pancreatic organoid. For the organoid there is an additional pie plot showing the cell type distribution excluding proliferating cells. **B.** UMAP of 4 cell types: progenitors, endocrine progenitors, endocrine cells and enteric nervous system (ENS) neuron and endocrine, coloured by cell types (right-hand side) and samples (middle). A summary of the percentage of endocrine cells in each sample (left-hand side). At the bottom, pie plots show the sample distribution in the clusters of the progenitors, endocrine progenitors and endocrine cells. The sample colour legend is presented in middle UMAP plot. **C.** Gene expression of selected genes projected on the UMAP plot. Colour intensity indicates level of expression. **D.** Expression dotplot of selected genes in each sample. The size of the dot corresponds to the percentage of cells expressing a gene in each cluster. The color represents the average expression level. **E.** Endocrine cell composition (clusters: endo. progenitors, endocrine and ENS neurons and endocrine) of double expression of either Gsk3b or Rbpj with the hormones Ins1, Gcg or Sst. 0,0 indicates neither expression of the 2

genes in a cell, 0,1 indicates no expression of Gsk3b or Rbpj and expression of the hormones (Ins1, Gcg or Sst) in a cell, 1,0 indicates expression of Gsk3b or Rbpj and no expression of the hormones (Ins1, Gcg or Sst) in a cell and 1,1 indicates double expression of the 2 genes in a cell.

The mesenchymal population was the dominant cell population in in the three embryonic pancreas datasets, whereas cluster 2, defined as a population of proliferating cells, was dominant in the organoid (Fig. 6A). Approximately 14% of the entire organoid had an endocrine identity (Fig. 6B), which is similar to the endocrine percentage in the embryonic samples at E14 (batch 1 with 24% and batch 2 with 11%) and E17 (20%, Fig. 6B). Upon exclusion of cluster 2 from the organoid dataset, the mesenchymal population became the larger (Fig. 6A) and an important endocrine compartment, composed of endocrine progenitors, endocrine cells and ENS neurons, was noted in the organoid (Fig. 6A).

In addition to the similarity in the endocrine proportion found in the two systems analysed (pancreatic organoid versus embryonic pancreas), the endocrine differentiation path was also comparable. The in vitro cells nicely projected onto the endocrine differentiation trajectory obtained in the UMAP plot (Fig.5D and Fig. 6B- C), from progenitors (Sox9) towards endocrine progenitors (Neurog3) and committed endocrine cells (Neurod1, Chga, Chgb). Although analysis of scRNA-seq data of the in vitro cells failed to detect hormones with the exception of Sst (Fig. 4B-C and Fig. 6D), immunostaining identified insulin and glucagon expressing cells (Fig. 3D and Fig. S4C). The failure to detect mRNA encoding hormones in the pancreatic organoid might be due to their lower expression levels or to the higher expression of three genes: Rbpj, a central regulator of Notch signalling, GSk3b, negative regulator of the Wnt pathway, and Insm1, a suppressor of Neurod1 and insulin-secreting cells (Fig. 6C-E). For example, almost all the cells that were positive for one of the three hormones, Ins1, Gcg or Sst, in the embryonic endocrine population at different stages of pancreas development were negative for Rbpj, but some were positive for Gsk3b. Moreover, the embryonic endocrine population contained very few cells positive for Rbpj (Fig. 6E). In contrast, most of the endocrine population in the pancreatic organoid was positive for Rbpj and Gsk3b, suggesting that Rbpj seemingly impaired full endocrine differentiation (Fig. 6E).

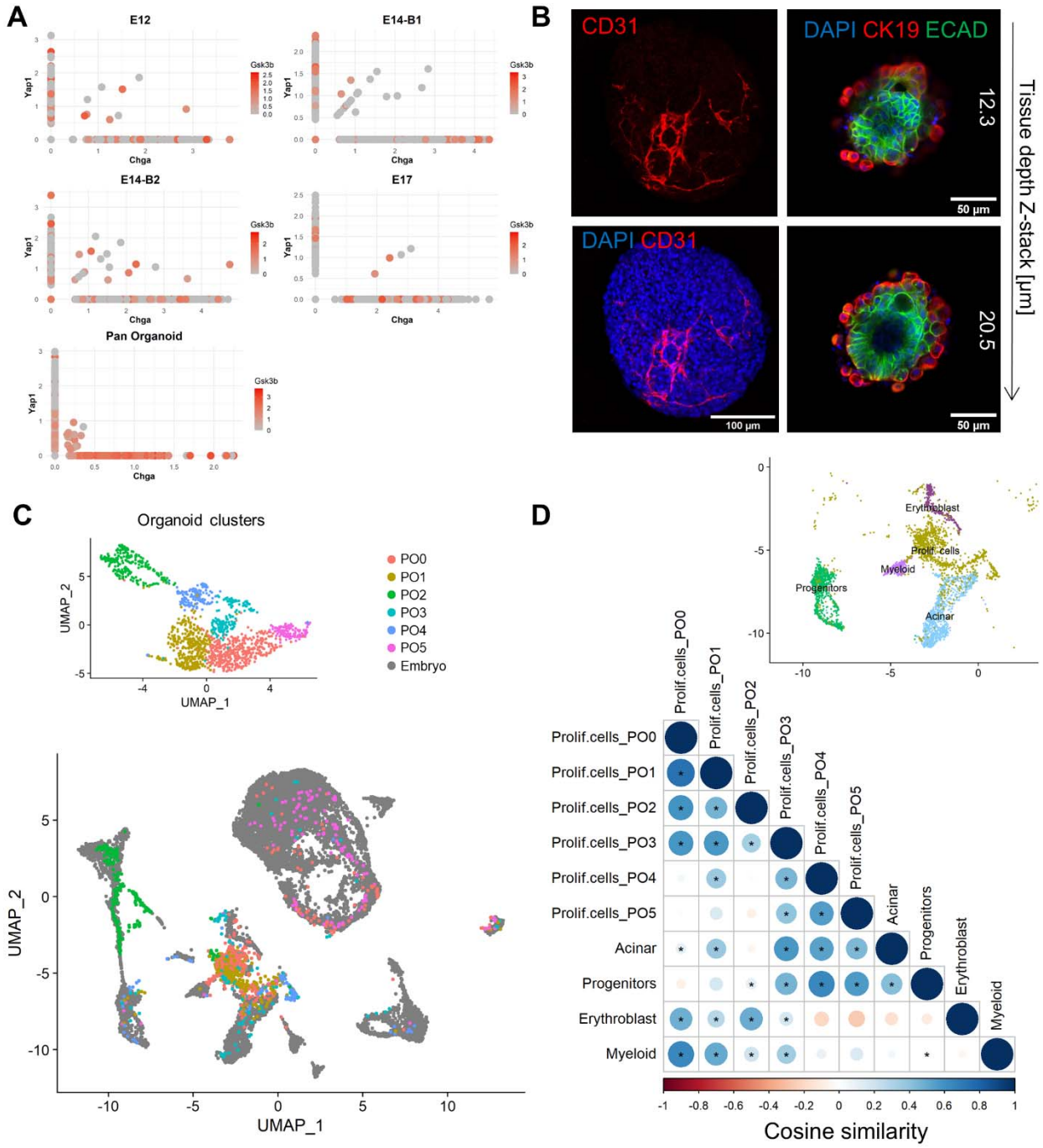

Figure 7. Pancreatic organoids do not lack mechanical cues to differentiate to hormone-producing cells and their major cluster composed from different embryonic cell types. A. Gene expression of Chga, Yap1 and Gsk3b in each sample. Each dot represents a cell, x and y axes show the normalized expression of Chga and Yap1, respectively. The normalized expression level of Gsk3b is indicated by the colour intensity. **B.** Confocal images of organoids embedded in 6.6% gelatin crosslinked with 5% microbial transglutaminase (mTG). The embedded organoid immunofluorescently stained for CD31 which marks the vessel-like network seen in the organoid (left), and for ECAD and CK19 (right) showing the epithelial and ductal regions at different tissue depths (Z-stacks) in the organoid. Nuclear staining with DAPI is in blue. **C.** Projecting the 6 pancreatic organoid clusters on the integrated UMAP plot. **D.** Cosine similarity score between the 6 organoid clusters comprising the proliferating cell group and

4 known cell types from the integrated data presented on the right: progenitors, acinar, myeloid and erythroblast. PO0 stands for pancreatic organoid cluster 0, PO1 stands for pancreatic organoid cluster 1, and so forth.

To test whether pancreatic organoids grown in suspension have less alpha and beta cells in comparison to the embryo, we first checked the relation between the expression of Yap1, Chga and Gsk3b (Fig. 7A). We thought that the absence of an outer support layer of the organoid might affect the mechanical signalling, hence perturbing the expression of the mechanoresponsive transcription factor Yap1. A recent work by Mamidi et al., 2018 suggests that extracellular cues inactivate Yap1, which triggers endocrinogenesis. In all samples, there was a negative relationship between Yap1 and Chga expression, indicating that Yap1 expression profile in the organoid is similar to that found in embryonic pancreas. However, endocrine cells from the pancreatic organoids expressed higher levels of Gsk3b in comparison to those from embryonic pancreas (Fig. 7A). Taken together, in our system, the higher expression level of Gsk3b might prevent endocrine cells from further differentiating into insulin- and glucagon-secreting cells, i.e., beta and alpha cells, respectively.

To further investigate whether growing pancreatic organoids in suspension can explain the difference with the in vivo endocrine differentiation, we embedded pancreatic organoid in 6.7% gelatin crosslinked with 5% microbial transglutaminase (mTg, Fig. 7B and Methods), an FDA-approved enzyme that makes covalent bonds between lysine and glutamine groups of proteins and gelatin polymers (Gupta et al., 2021; Paguirigan and Beebe, 2007; Yung et al., 2007). Gelatin-mTG hydrogel was used here for organoid encapsulation, providing it with mechanical support, but also because this gelatin-mTG hydrogel has been shown to improve cell maturation and long-term culture (Gupta et al., 2021; McCain et al., 2014; Yung et al., 2007). The gelatin-embedded pancreatic organoids contained a CD31-positive vessel-like network and contained ductal regions marked by ECAD and CK19 (Fig. 7B and Video S1). However, we could not detect insulin- or glucagon-expressing cells, suggesting that mechanosignalling was not a limiting factor minimizing in vitro formation of hormone-producing cells.

Unique in vitro populations that share similarities with the embryo

The proliferating cell cluster (cluster 2) is a distinct cluster of the pancreatic organoid which scarcely contained embryonic cells. The identity of this cluster was not clear and the signalling pathways discrepancy between the organoid and the embryonic pancreas, mainly of Notch and Wnt, might explain the difference between the organoid and embryonic pancreas. Nevertheless, the integrated UMAP plot showed proximity between cluster 2 and other known cell types (Fig. 5D, Fig. 7C-D), alluding to its obscure identity. The 6 clusters found in the pancreatic organoid were projected on the organoid-embryo integrated UMAP plot (Fig. 7C). Proliferating cell cluster contained cells from these 6 pancreatic organoid clusters (Fig. S7A) and was surrounded by erythroblast, myeloid and acinar clusters, and some of its cells were projected on the progenitor cluster on the UMAP plot (Fig. 7D). Hence, we wished to assess the similarity between the 6 pancreatic organoid clusters in the proliferating cluster and these known cell types (Fig. 7C-D and Fig. S7). We first calculated the mutual information (MI) between expression of all the genes and cell assignment to 5 clusters (proliferating cells, progenitors, erythroblast, myeloid and acinar clusters). Only genes with MI≥0.2 (Fig. S7B) were used to calculate the cosine similarity between the 6 organoid clusters in the proliferating cell group and the 4 known clusters (Fig. 7D and methods). Proliferating cell cluster was comprised of mixed populations, including pancreatic organoid cluster 0 (PO0), which resembled the myeloid and erythroblast cells, PO1, which was most similar to myeloid cells and displayed similarity to erythroblasts, PO2, which was mainly similar to erythroblast cells, PO3, which resembled the acinar group and exhibited positive similarity to

the progenitor group, PO4, which had high similarity to the progenitor group and slightly less to the acinar cells and PO5, which had profile similar to that PO4, but its values were slightly lower (Fig. 7D). The cluster cosine similarity profile of the organoid was in correspondence with the in vitro cell positions in the UMAP (Fig. 7C-D). Specifically, we observed that mainly PO4 and cells from PO5 were located at the progenitor cluster position of the integrated UMAP (Fig. 5D and Fig. 7C-D), suggesting that they could be in vitro progenitors.

Discussion

In this study, a well-defined in vitro culture system of mESC-derived progenitors was designed to mimic development of mouse embryonic pancreas. The first step relied on differentiation of mESCs to PPs adapted from human ESC differentiation to PPs (Hohwieler et al., 2017). The main changes in the differentiation protocol were the removal of Matrigel and advancing mESCs to epiblast state before differentiation. We noted that the initial pluripotency state of the cells (2i, SL and EpiSCs) prior differentiation determined the capacity of the cells to differentiate to definitive endoderm and dictated the subsequent PP differentiation yield. As compared to mESCs grown in 2i and SL prior differentiation, EpiSCs exhibited higher Sox17 expression at the DE stage and had a PP differentiation yield of approximately 90%, as determined by the coexpression of Pdx1 and Nkx6-1 and other pancreatic genes. This yield was remarkable compared to previously reported yields of 70% or less, even after a cell sorting step (Borowiak et al., 2009; Chen et al., 2009; Delaspre et al., 2013; Hohwieler et al., 2017; Mamidi et al., 2018). Furthermore it emphasized the responsiveness of EpiSCs to activin and their vast capacity to commit to DE, which is a major step in ensuring a successful PP differentiation protocol (Lee and Chung, 2011).

After establishing a reproducible protocol for PP production, we set out to mimic the 3D pancreatic microenvironment of the mouse developing pancreas. To this end, EpiSC-derived pancreatic and mesodermal progenitors were mixed in proportions similar to those measured in the embryo (Glorieux et al., 2022) to form an aggregate. The MPs supplied the PPs with mesodermal cues, but also cellular interactions via specialized cell types, such as endothelial and mesenchymal cells, which are essential for pancreas differentiation and maturation in vivo. It has been shown that growing progenitors on organ-matched mesenchyme elicits their expansion and self-renewal and, importantly, gives rise to glucose-sensing and insulin-secreting cells when transplanted in vivo (Sneddon et al., 2012). Here, aggregation of EpiSC-derived PPs with EpiSC-derived MPs without the use of Matrigel, resulted in a pancreatic organoid containing a range of cell types: progenitors, epithelial, acinar, endocrine, mesenchymal and endothelial cells. Moreover, insulin and glucagon expression was detected in immunostaining analyses, indicating the presence of beta and alpha cells, respectively.

scRNA-seq extended the depth of the organoid analysis and revealed the diverse cell populations that existed in the pancreatic organoid. Some discrepancies were found between the immunofluorescence staining results and the scRNA-seq data, mainly related to insulin and glucagon, which were not detected at the mRNA level. This may be the result of pooling of single cells from hundreds of organoids for the scRNA-seq analysis, which might interfere with the detection of rare cell types and genes expressed at low levels, e.g., hormone-secreting cells.

Single-cell resolution of the organoid transcriptome enabled its comparison with published transcriptomic data of mouse embryonic pancreas. Embryonic datasets at E12, E14 and E17 demonstrated that the pancreatic organoid culture system succeeded in recapitulating many of the cell populations residing in the pancreas, including small populations, such as endothelial cells. Furthermore, the organoid had an endocrine compartment profile similar to that of the E14 and E17 pancreas and endothelial compartment similar to that of the E14 pancreas. Resemblance to the embryonic pancreas was not only in the relative size of the endocrine population but also in the differentiation path of the

progenitors to mature endocrine cells. Yet the pancreatic organoid did not entirely mirror the embryo and contained a population (cluster 2) that was distinct from the embryonic pancreatic cells. Although this population was mainly composed of pancreatic organoid cells that did not cluster with the embryonic pancreatic cells, they exhibited a gene profile that was close to known clusters (myeloid, erythroblast, acinar and progenitors) from the integrated data. This discrepancy between the pancreatic organoid cells and the in vivo cells, indicating some differences between the populations. The gap between cells from the pancreatic organoid and the embryonic pancreas might reflect differences in the main signalling pathways driving pancreas development, i.e., Notch, Wnt and Hippo pathways. A recent work of Mamidi et al., 2018 suggested that extracellular cues inactivate Yap1, which triggers endocrinogenesis. In our in vitro system, although the organoid was grown in suspension and lacked the mechanical support usually provided by Matrigel, most of the cells that were positive for Chga were also negative for Yap1, indicating that the in vitro progenitors can produce endocrine cells. The endocrine cells of the pancreatic organoid also expressed higher level of Gsk3b, a Wnt repressor, and of Rbpj, a central regulator of Notch signalling, in comparison to the embryo. Notch signalling helps maintain progenitor proliferation and prevents premature differentiation to ductal and endocrine fate (Li et al., 2016; Wu et al., 2021). Wnt signalling regulates pancreatic specification and patterning during different stages of pancreas development (McCracken and Wells, 2012; Wu et al., 2021). On the one hand Wnt inhibition is necessary for endocrine differentiation (Sharon et al., 2019b), but on the other hand deletion of Wnt-related genes has been found to reduce the proportion of pancreatic progenitors, which subsequently reduces the number of both endocrine and exocrine cells (Wu et al., 2021). In light of an earlier report that Gsk3b overactivation results in decreased pancreatic beta cell proliferation and mass (Liu et al., 2008) and that high levels of Notch signalling lead to the repression of Neurog3, preventing endocrine cell fate determination (Wu et al., 2021), we propose that, in our system, Gsk3b and mainly Rbpj limit endocrine cells from further differentiating into insulin- and glucagon-secreting cells. Overall, the transcriptomic analyses revealed the similarities and differences between the pancreatic organoid and the mouse embryonic pancreas and highlighted signalling pathways and mechanisms that may govern pancreas progenitor differentiation and development.

To further determine whether the lack of mechanical cues generally provided by Matrigel, prevented the emergence of insulin- and glucagon-producing cells in the in vitro system, we embedded the pancreatic organoid in a gelatin-mTG hydrogel, with the aim to constrain cells in space. However, cells positive for insulin or glucagon were not detected in the gelatin-embedded organoids, suggesting that pancreatic organoid confinement in hydrogels does not help producing beta and alpha cells. This implies that mechanical cues are either already present via the MP counterpart of the organoid or that they are not the key determinant of full endocrine differentiation in this pancreatic organoid model. Nevertheless, the gelatin-embedded organoids were highly vascularized and displayed epithelial ductal regions, which are important for in vitro maturation and indicate correct development. Achieving of such organoid vascularization shows advancement in tissue engineering field, since vascularization is important for organoid growth, prevents necrosis as they increase in size and prevents premature differentiation (Grebenyuk and Ranga, 2019).

Until recently, the study of embryo and organ development has been restricted to animal embryos and and fetal tissues. These models and material sources are limited and their use presents ethical concerns. The increasing utilization of human and mouse stem cell-derived organoids has significantly expanded the study of mammalian development and promoted regenerative and therapeutic medicine, whilst reducing the use of animals. Nevertheless, most organoids and specifically pancreatic organoids rely on

the use of Matrigel, failing to achieve a reproducible and fully defined in vitro 3D system. Our study aimed to maximize in vitro resources to construct a new in vitro system based on mixing endoderm- and mesoderm-derived progenitors in a defined proportion. In future this proportion can be explored in the in vitro system, which might teach us about the important interaction between the endoderm- and mesoderm-derived progenitors. The novel system closely recapitulated key elements of mouse embryonic pancreas and bears the potential to serve as a model that all parameters can be tuneable to study mammalian pancreas development and pancreas diseases.

Methods

Cell culture

ES-E14TG2a (ATCC CRL-1821) mouse embryonic stem cells (mESCs) were grown in sterile flasks pre-coated with 0.1% porcine skin Type A gelatin (Sigma-Aldrich, G1890) in pluripotency medium referred to as serum and LIF (SL), comprised of GMEM (Gibco) supplemented with 1% non-essential amino acids (100X Gibco), 1mM sodium pyruvate (Biological Industries), 1% GlutaMAX (100X Gibco), 0.1mM β-mercaptoethanol (Gibco), 10% foetal bovine serum (FBS) (HyClone, Thermo Fisher Sceintific), and 10ng/ml LIF (R&D systems). Cells were maintained at 37°C in 5% CO_2. Medium was changed daily, and cells were passaged with trypsin (Biological Industries) every 2-3 days, as necessary, up to a total of 30 passages.

2i

2i was comprised of basal differentiation medium NDiff®227 (Takara), hereby referred to as N2B27, supplemented with 1µM MAPK inhibitor PD0325901 (Sigma-Aldrich, referred as PDO3) and 3µM GSK3β inhibitor CHIR99021 (Sigma-Aldrich, referred to as Chiron). Cells grown in 2i medium are in a stringent pluripotency environment and are considered to be at ground-state pluripotency (Ying et al., 2008).

Epiblast stem cell and Epi-medium

ES-E14TG2a were grown in plastic tissue-culture flasks coated with 5µg/ml plasma fibronectin (F0895, 1 mg/ml, Sigma-Aldrich) in Dulbecco's phosphate-buffered saline (DPBS with calcium and magnesium, Sigma-Aldrich, D8662). mESCs were grown in Epi-medium: N2B27 (NDiff®227, Takara) supplemented with 12ng/ml FGF2 (Peprotech) and 25ng/ml Activin A (Peprotech), for at least four passages, to generate EpiSCs (Edri et al., 2019a).

Differentiation of mESCs to pancreatic progenitors (PPs)

The differentiation protocol below is a variation of one previously used to derive PPs from human pluripotent stem cells (Hohwieler et al., 2017). Prior to differentiation, mESCs were grown in either SL, 2i or as EpiSCs in Epi-medium. Cells grown in SL and 2i were grown in sterile flasks pre-coated with 0.1% gelatin, whereas flask with EpiSCs were pre-coated with 5µg/ml fibronectin.
Cells were plated at a density of $5x10^4$ cells/cm^2 in their respective growth medium (SL, 2i or Epi-medium) 24 h prior to differentiation (day 0). The backbone medium for the first 5 days of differentiation was BE1: MCDB131 (Gibco) supplemented with 0.8g/L cell-culture-tested glucose (Sigma-Aldrich), 1.174g/L sodium bicarbonate (Biological Industries), 0.1% fatty acid-free (FAF) BSA (Sigma-Aldrich) and 2mM GlutaMAX. The backbone medium for the subsequent 9 days of differentiation was BE3: MCDB131 supplemented with 0.44g/L glucose, 1.754g/L sodium bicarbonate, 2% FAF-BSA, 2mM GlutaMAX, 4.4mg/L-ascorbic acid (Sigma-Aldrich) and 0.5x insulin-transferrin-selenium-ethanolamine (Gibco). Cells undergoing differentiation were cultured at 37°C in a 5% CO_2 incubator and medium was changed daily. On day 1, cells were washed with DPBS and incubated with BE1 supplemented with 3µM Chiron (CHIR99021, Sigma-Aldrich) and 100ng/mL activin A. On day 2, medium was replaced by BE1 with 100ng/mL activin A for 2 days. On day 4, medium was changed to BE1 with 50ng/mL keratinocyte growth factor (KGF also known as FGF7, Peprotech) for 2 days. On day 6-9, cells were cultured in BE3 medium containing 0.25µM SANT-1 (Sigma-Aldrich), 2µM retinoic acid (Sigma-Aldrich), 200nM LDN-193189 (Sigma-Aldrich) and 500nM PDO3 (PD0325901 Sigma-Aldrich). On days 10–14, the cells received BE3 supplemented with 50ng/mL FGF10 (R&D systems), 330nM Indolactam V (Cayman), 10µM SB431542 (Tocris) and an additional 16mM glucose. An outline of the differentiation protocol can be found in Fig. 1A.

Mesoderm progenitors (MPs)

The differentiation protocol of EpiSCs to mouse embryo caudle epiblast (CE)-like cells is detailed in (Edri et al., 2019a, 2019b). Briefly, EpiSCs were differentiated to Epi-CE, which resemble the caudle epiblast of the mouse embryo and contain the different mesoderm compartments: lateral plate mesoderm, intermediate and paraxial mesoderm, hence we refer these cells here as mesoderm progenitors. EpiSCs were plated at a density of 5×10^4 cells/cm^2 in a flask pre-coated with 5µg/ml fibronectin and grown in Epi-media for the first day (day 0). On Day 1, medium was replaced with N2B27 base medium with 20 ng/ml FGF2 and without activin A. On day 2, N2B27was supplemented with 3µM Chiron and 20ng/ml FGF2.

Organoid preparation

PPs and MPs in adherent culture were dissociated from culture flasks with accutase (STEMCELL Technologies) on days 14 and 3 of differentiation, respectively. Cells (n=1000) at a ratio of 58% PPs and 42% MPs were plated in each well of a U-bottom 96-well plate in 50µL organoid medium composed of Dulbecco's Modified Eagle Medium/Nutrient Mixture F-12 (DMEM/F-12(HAM)1:1, Biological Industries) with 10% knockout serum replacement (KSR, Gibco), 1% penicillin-streptomycin (PS, Biological Industries), 0.1mM β-mercaptoethanol (Gibco), 16nM phorbol myristate acetate (PMA, Sigma-Aldrich), 5µM ROCK inhibitor (Thazovivin, Sigma-Aldrich), 25ng/mL epidermal growth factor (EGF, Sigma-Aldrich), 500ng/ml mouse R-spondin1 (R&D systems), 2.5U/mL heparin sodium salt (Sigma-Aldrich), 25µg/mL acidic fibroblast growth factor (aFGF, R&D systems), and 100ng/mL FGF-10 (Greggio et al., 2013). After 48 h, 100µL of the same medium was added to each well for an additional 48 h. On day 4 after aggregation (AA) the organoids were transferred to a 6 well-plate and placed on an orbital shaker at 110 RPM (RCF of 0.11808g and shaking diameter of 10mm) for an additional 4 days (total 22 days of differentiation, Fig. 3B). Wells were supplemented with 3ml organoid medium, which 1ml was changed every 2 days from day 4 AA until the end of differentiation.

Organoid cell ratio justification: At embryonic stages E12.5 and E14.5, the pancreas was composed of 58% epithelial cells, 37% mesenchymal cells and 5% endothelial cells (Fig. 5C in (Glorieux et al., 2022)). Mesoderm gives rise to mesenchyme, endothelium and blood cells (Ghezelayagh et al., 2021; Talavera-Adame, 2015), hence MPs represent the mesenchymal and endothelial cells and PPs represent the epithelial compartment of the pancreas embryo, resulting in a ratio of 58% PPs and 42% MPs in an aggregate (Fig. 3A).

RNA extraction and real-time quantitative polymerase chain reaction (RT-qPCR)

RNA was extracted at different time points during EpiSC differentiation to PPs using the RNeasy extraction kit (Qiagen), according to the manufacturer's instructions. RNA concentration was measured with a NanoDrop (NanoDrop One, Thermo Fisher Scientific). cDNA was synthetized using the high-capacity cDNA Reverse Transcription Kit (Applied Biosystems, Thermo Fisher Scientific), according to the manufacturer's instructions. RT-qPCR was performed using Fast SYBR Green Master Mix (Applied Biosystems, Thermo Fisher Scientific), according to the manufacturer's instructions. The gene-specific primers that were used are shown in Table 1. The reaction was performed in a QuantStudio1 (Applied Biosystems, Thermo Fisher Scientific), in technical triplicates. All experiments were performed in biological triplicates. Expression values were normalized against the housekeeping gene Ppia ($2^{-\Delta ct}$). The results are presented as the average across biological replicas ($2^{-mean(\Delta ct)}$) with the standard error of the mean (SEM, $2^{-(mean(\Delta ct)\pm sem(\Delta ct))}$).

Table 1. qPCR primer list

Gene	Forward primer	Reverse primer
Ppia	TTACCCATCAAACCATTCCTTCTG	AACCCAAAGAACTTCAGTGAGAGC
Nanog	CCTCCAGCAGATGCAAGAA	GCTTGCACTTCATCCTTTGG
Sox2	CATGAGAGCAAGTACTGGCAAG	CCAACGATATCAACCTGCATGG
Oct4	CCAATCAGCTTGGGCTAGAG	CTGGGAAAGGTGTCCCTGTA
Fgf5	TGGCATTATGTGGAATCTGG	CTGTGGACGCTGCACACTT
Sox17	GTAAAGGTGAAAGGCGAGGTG	GTCAACGCCTTCCAAGACTTG
Foxa2	CATTACGCCTTCAACCACCC	GGTAGTGCATGACCTGTTCG
Ecad	CAATGCCTGCTCTTGATGGT	GGGAGATCTGACTGCCTCTG
Pdx1	CATCGCGCCACTGCGAC	TTTCTTCTTGTGCGACGCC
Nkx6-1	AACACACCAGACCCACGTTC	GAACCAGACCTTGACCTGACTC
Sox9	AGACTCACATCTCTCCTAATGCT	ACGTCGGTTTTGGGAGTGG
Ptf1a	AGGTTATCATCTGCCATCGAG	GACACAAACTCAAAGGGTGGT
Pax6	AAGCACTTCACTTTGTAACTGTCC	CCAACTGATACCGTGCCTTC
Insm1	GCCCAGGTGTTCCCCTGCAA	AGGCCCGGGGAGCTGTAGAA

Immunofluorescence and confocal imaging

Cells and organoids were washed with phosphate-buffered saline (PBS) 1X (Gibco) and fixed in 4% paraformaldehyde (PFA) (ChemCruz, Santa Cruz Biotechnology) for 15 min at room temperature (RT). Samples were washed and permeabilized for 15 min with PBST: PBS 1X + 1mM $CaCl_2$, supplemented with 0.5% bovine serum albumin (BSA) (Millipore) and 0.5% Triton X-100 (Bio-Lab Ltd.) before overnight incubation at 4°C with primary antibodies diluted in PBST. Antibody details are shown in Table 2. The following day, samples were washed with PBST and incubated at room temperature for 2 h with secondary antibodies and 4′,6-diamidino-2-phenylindole (DAPI) (Sigma-Aldrich) diluted in PBST. Samples were washed with PBS 1X and stored in fresh PBS 1X at 4°C until imaging. Organoids were mounted on microscope slides by pipetting them in 15ul droplets of Fluoromount-G (SouthernBiotech, 0100-01). A microscope cover glass (No. 1.5H 24 mm x 60 mm) with an adhesive spacer (Silicone isolators, press-to-seal, Sigma-Aldrich) was placed on the slide with the organoids.
Cells and organoids were imaged using a confocal microscope (LSM700, Ziess) and Fiji software (ImageJ) was used to process and analyse the images.

Table 2. Primary and secondary antibodies used in this study

Antibody	Dilution	Manufacturer
Rabbit anti PDX1	1:2200	ab47267 Abcam
Guinea pig anti PDX1	1:500	ab47308 Abcam
Mouse anti NKX6-1	1:400	F55A12-c DSHB
Mouse anti Sox9	1:500	SC-166505 Santa Cruz
Goat anti Sox17	1:200	AF1924 R&D
Rat anti Ecad	1:200	U3254 Sigma-Aldrich
Mouse anti Neurogenin3 (C-7)	1:500	SC-374442 Santa Cruz
Mouse anti Amylase	1:200	SC-46657 Santa Cruz
Rabbit anti ERG	1:500	ab92513 Abcam
Mouse anti glucagon	1:1000	G2654 Sigma-Aldrich
Guinea pig anti insulin	1:200	A0564 DAKO
Goat anti NeuroD1	1:300	AF2746 R&D
Rabbit anti Cytokeretin19 (CK19)	1:500	ab133496 Abcam
Rabbit anti Cdx2	1:500	ab76541 Abcam
Rabbit anti Tbx3	1:100	ab99302 Abcam
Rabbit anti Vimentin	1:1000	ab92547 Abcam

Rat anti CD31	1:50	550274 BD Biosciences
Donkey anti rat Alexa fluor 488	1:400	ThermoFisher Scientific
Donkey anti guinea pig Alexa fluor 488	1:200	Jackson Immunoresearch Laboratory
Donkey anti goat Alexa fluor 488	1:400	ThermoFisher Scientific
donkey anti-mouse Alexa fluor 488	1:400	ThermoFisher Scientific
Donkey anti guinea pig Alexa fluor Cy3	1:500	Jackson Immunoresearch Laboratory
Donkey anti mouse Cy3	1:400	Jackson Immunoresearch Laboratory
Donkey anti rabbit Cy3	1:400	Jackson Immunoresearch Laboratory
Goat anti Rat Alexa fluor 647	1:400	ThermoFisher Scientific
Donkey anti rabbit Alexa fluor 647	1:400	ThermoFisher Scientific
Donkey anti-mouse Alexa fluor 647	1:100	Jackson Immunoresearch Laboratory
Donkey anti-rat Cy5	1:200	Jackson Immunoresearch Laboratory

Flow cytometry

Flow cytometry was performed to assess the differentiation of EpiSCs to PPS on day 14 using mouse anti-NKX6-1 and rabbit anti-PDX1 antibodies (Table 2). EpiSC-derived PPs were fixed in 4% PFA for 15 min. Cells were centrifuged at RT for 3 min at 300 *g* to remove the fixation solution, and then washed in PBST. The cells were incubated with PDX1 and NKX6-1 primary antibodies overnight at 4°C. The following day, the cells were centrifuged at RT for 5 min at 300g, washed in PBST and centrifuged at RT for 5 min at 300g. Next, the cells were incubated with donkey anti-mouse Alexa fluor 647 (1:100, Jackson Immunoresearch Laboratory) and donkey anti-rabbit Cy3 (1:400, Jackson Immunoresearch Laboratory) secondary antibodies for 2 h at RT, in the dark. Cells were washed in PBST, centrifuged at RT for 5 min at 300g and resuspended in PBS 1X. Control samples were incubated with secondary antibodies only. Cells were analysed using the BD FACS Aria-IIIu cell sorter (BD) and the data were assessed with FlowJo analysis software (BD).

Single-cell RNA sequencing (scRNA-seq)

On day 22 (day 8 AA), pancreatic organoids were dissociated into single cells with accutase and 10x Genomics single cell transcriptomic service was used to sequence the cells. Single-cell RNA sequencing libraries were generated for 3,121 pancreatic organoid cells. Briefly, after applying various filtering steps, a total of 1475 cells were retained for subsequent analysis. To group cells into perspective cell types we used graph-based clustering R package Seurat v4.0.6 (Hao et al., 2021) followed by visualization using Uniform Manifold Approximation and Projection (UMAP) dimensionality reduction technique, which revealed 6 clusters.

Library preparation and data generation

One RNA single-cell library was prepared according to the 10x manufacturer's protocol (Chromium Next GEM Single Cell 3' Library & Gel Bead Kit v3.1, PN-1000121) at the Technion Genomics Centre. Single-cell separation was performed using the Chromium Next GEM Chip G Single Cell Kit (PN-1000120). The RNA-seq data was generated on Illumina NextSeq2000, P2 100 cycles (Read1-28; Read2-90; Index1-10; Index2-10) (Illumina, cat no. 20046811). Cell Ranger version 6 (10x Genomics) was used to process raw sequencing data and the Seurat R package version 4.0.6 (Hao et al., 2021) was used to build the expression matrix. Gene expression was quantified by unique molecular identifiers (UMI) counts.

Mouse embryo single-cell RNA-seq data

The single-cell transcriptomic data of pancreatic organoids was compared to transcriptomic data of the mouse pancreas from embryonic days 12, 14, and 17 (Byrnes et al., 2018). As detailed by Byrnes et al. (Byrnes et al., 2018) single-cell RNA-sequencing libraries were generated for 4,631 cells at E12, 9,028 cells at E14 (comprised of two independent batches E14_B1 and E14_B2), and 4,635 cells at E17. Cell and gene filtering, normalization and data integration between the organoid and the embryo samples were all performed with R package Seurat, version 4.0.6 (Hao et al., 2021).

Single-cell data clean up and quality control

Using Seurat V3 R package, version 4.0.6 (Hao et al., 2021), the expression matrix was cleaned in the 4 following aspects: 1) UMI counts: only cells that had 500-70,000 UMI counts were retained for further analysis, ensuring a sufficient sequencing depth for each cell. 2) Detected genes: only cells that have 500-7000 unique genes in a cell were retained for further analysis, to ensure that the reads were distributed across the transcriptome. 3) Mitochondrial gene expression: an upper limit of 20% mitochondrial genes (mitochondrial gene counts in a cell versus the total detected genes in a cell) in a cell was set, to reduce the likelihood that cells for further analysis were dead or stressed. 4) Gene filtering: a threshold of at least 5 cells containing more than 1 UMI of a gene was set. The number of cells and total genes after the clean-up are presented in Table 3. The organoid data was processed with Seurat V3. First, the expression matrix was log-normalized and then scaled (linear transformed) that the mean and the variance expression of each gene across cells is 0 is 1 respectively. Next, principal component analysis (PCA) was performed, from which the first 28 principal components (PCs) were selected for uniform manifold approximation and projection (UMAP) analysis and cell clustering, which is a graph-based clustering approach. Integration of the in vivo and in vitro samples was performed using the Seurat V3 anchoring method (Hao et al., 2021). The integrated expression matrix was log-normalized and scaled. Next, PCA was performed and the first 30 PCs were selected for UMAP analysis and cluster finding.

Marker genes for all clusters was detected as genes with at least Log2(fold change) ≥1 and adjusted p-value ≤0.05 (Table S2). The GSEA MSigDB (https://www.gsea-msigdb.org/gsea/msigdb/) and Descartes (https://descartes.brotmanbaty.org/bbi/human-gene-expression-during-development/dataset/pancreas) databases were used to help assign identities for the 23 clusters according to their marker genes.

Table 3. The number of cells in each sample and the total number of detected genes after data clean up.

	Cell number	Gene Number
E12	4,412	18,426
E14_B1	3,495	18,426
E14_B2	4,309	18,426
E17	2,241	18,426
Pan Organoids	1,475	18,426

Mutual information between genes and clusters

To characterize cluster 2, which was named 'proliferating cells', the similarity between the organoid cells in cluster 2 and its surrounding 4 clusters of known identity (progenitors, erythroblast, myeloid, and acinar clusters) on the UMAP plot, was assessed. Downstream analysis was implemented with the whole

set of qualified genes (18,426) rather than with the genes restricted to the integration process (2,000 anchor genes). This step was performed as previously detailed (Edri et al., 2019b; Vanitha et al., 2015). A mutual information (MI) technique (Battiti, 1994) was used to select the informative genes related to the 5 clusters (progenitors, proliferating cells, erythroblast, myeloid, and acinar clusters). The MI between the clusters (denoted as Y) and genes (denoted as X) was computed as follows:

1. Calculation of cluster entropy:
$$(1)\ H(Y) = -\sum_{y=1:5} p(y)\log_2\big(p(y)\big),$$
where $p(y)$ is the probability of each cluster $y = 1, 2, 3, 4, 5$.

2. Discretization of the gene expression values into ten bins and calculation of the conditional entropy $H(Y|X)$ as follows:
$$(2)\ H(Y|X) = \sum_x p(x)H(Y|X = x)\ ,$$
where $p(x)$ is the probability of the discretized gene expression across the cell population and $H(Y|X = x)$ is the cluster entropy given a specific gene expression value, calculated following Equation 1.
3. Computation of the MI between the clusters and each gene according to the equation below:
$$(3)\ MI(X;Y) = H(Y) - H(Y|X)$$
4. Setting of a threshold of the MI of all the genes and selection of the informative genes above this value (Fig. S6G).

Fig. S7B shows the MI between the genes and the clusters versus the number of genes. We set MI=0.2 since at this point, the MI value was almost unfluctuating with increments in gene number. This threshold, in which genes have MI above or equal to 0.2 (190 genes in total, Table S3), determines which genes are selected as input features for calculating the cosine similarity.

Cosine similarity

Cosine similarity was used as a measure of similarity between gene expression of the informative 190 genes selected by MI in one cluster versus another cluster. The cosine similarity was calculated as follows:

$$similarity = \frac{\sum_{i=1}^{n} A_i B_i}{\sqrt{\sum_{i=1}^{n} A_i^2}\sqrt{\sum_{i=1}^{n} B_i^2}},$$

where A and B represent two clusters and A_i and B_i are the gene expression values in each condition (n=190). Similarity of -1 indicates that the conditions are opposite and 1 indicates maximal similarity.

Organoid embedding in gelatin

Gelatin hydrogel was covalently crosslinked with microbial transglutaminase (mTG) (MOO gloo TI transglutaminase, SKU:1203-50, modernist pantry) in the presence of calcium ions (Gupta et al., 2021). Porcine skin gelatin (300g Bloom type A, Sigma-Aldrich, G1890) was dissolved in PBS 1X at 50°C and immediately passed through a 0.22µm filter. mTG was dissolved in 10mM HEPES buffer (Biological Industries) supplemented with 100mM $CaCl_2$ and sterilized through a 0.22µm filter.
On day 6 AA, pancreatic organoids were embedded with 6.7% gelatin and 5% mTG, prewarmed to 37°C. Plugs (50µl) of gelatin-mTG with organoids were pipetted into wells of a 24-well plate. To solidify the gelatin, the plate was incubated for 10 min at RT, followed by 30 min at 37°C before adding the organoid medium.

Supplementary

Table S1. Key genes expression in the pancreatic organoid

Gene name	Function	Comments
Dll1	Notch pathway	
Vim	Mesenchymal and EMT marker	
Igfbp2	Insulin-like growth factor binding protein 2, EMT inducer in pancreatic ductal adenocarcinoma (Gao et al., 2016). Expressed in mesothelial cells in E12.5 and E17.5 mouse pancreas (Byrnes et al., 2018)	
Irx1	Differentiation regulators of alpha cells (Byrnes et al., 2018)	
Yap1	Hippo pathway	
Epcam	Pancreatic epithelium (Byrnes et al., 2018)	
Rbpj	Notch pathway	
Id2	Id DNA-binding protein family. Expressed in mesenchymal population in the mouse embryo pancreas (Byrnes et al., 2018)	
Hes1, Hes5	Notch pathway	
Ptn	Heparin-binding cytokine, expressed in interepithelial and delaminating Ngn3 + cells (EMT) in E14.5 mouse pancreas (Scavuzzo et al., 2018)	
Egr1	Expressed in endocrine progenitors and beta cells in E16.5 mouse embryo (Scavuzzo et al., 2018)	
Cxcl12	Chemokine expressed in mesenchymal cells in E14.5 mouse pancreas (Byrnes et al., 2018)	
Twist1	Delamination and migration markers	
Col3a1	Mesenchymal cells (Byrnes et al., 2018)	
Pdgfrb	Mesenchymal cells in the mouse embryo pancreas (Hori et al., 2008) and expressed in pericytes, which support the formation and maturation of blood vessels (Ranjan et al., 2009).	
Tcf4	Transcription factor in Wnt pathway	

Barx1	Mesenchymal cells	Few cells
Bmp7	Exocrine progenitors	41 cells
Col1a1	Mesenchymal cells in E14.5 mouse pancreas (Byrnes et al., 2018)	
Spp1	Ductal and proliferating ductal cells in E14.5 mouse pancreas (Byrnes et al., 2018)	
Ptf1a	Exocrine progenitors	
Mecp2	Methyl binding protein, expressed in beta cells (Arda et al., 2013; Quilichini and Haumaitre, 2015)	
Atf2	Beta cells (Byrnes et al., 2018)	
Sst	Delta cells	36 cells
Cdh2 (Ncad)	Cell adhesion molecule, required to establish the dorsal pancreatic mesenchyme (Seymour and Serup, 2019). Plays a role in cell-to-cell junction formation between pancreatic beta cells and neural crest stem cells. Expressed in mesoendodermal cells (Prabakar et al., 2012)	
Onecut1	Pancreatic progenitors	
Pecam1	Endothelial cells	7 cells
Sox4	Early endocrine progenitors (Scavuzzo et al., 2018)	
Insm1	Endocrine progenitors. Suppresses Neurod1 and insulin-secreting cells	
Myt1	Endocrine progenitors	
Stmn2, Stmn3	Regulator of microtubule stability. Stmn2 is expressed in alpha cells.	
Chga, Chgb	Endocrine cells	
Peg10	Mainly alpha but also beta cells (Byrnes et al., 2018)	
Hoxb4, Hoxd4		
Hoxb6, Hoxc6		
Hoxc10		
Gng12	Mainly beta, bet also alpha (Byrnes et al., 2018)	
Itga6	Exocrine cells: epithelial duct cells.	
Muc1	Ductal cells	9 cells
Rbp1	Cellular retinol-binding protein type I,	
Pax6	Pancreatic progenitors, endocrine progenitors, and beta cells.	

Crabp1	Cellular retinoic acid binding protein I, expressed in endocrine and exocrine glands.	
Cyp26b1	Involved in the metabolism of retinoic acid. Play a role in pancreas development.	
Top2a	Proliferating acinar and ductal cells	
Foxm1	Beta cells	
Ccnd2, Ccnd1, Ccnb2, Ccna2	Cyclin genes, proliferating cells and endocrine cells (Byrnes et al., 2018; Georgia et al.; Kim and Rane, 2011; Kushner et al., 2005)	

Table S2. Marker genes of the 23 clusters of the integrated organoid-embryo data

Table S3. List of genes with MI ≥0.2

Table S4. Endothelial compartment in each sample

	E12	**E14.B1**	**E14.B2**	**E17**	**Pancreatic organoid**
Endothelial cells out of total sample in percentage	0.63%	0.92%	1.04%	4.6%	0.95%

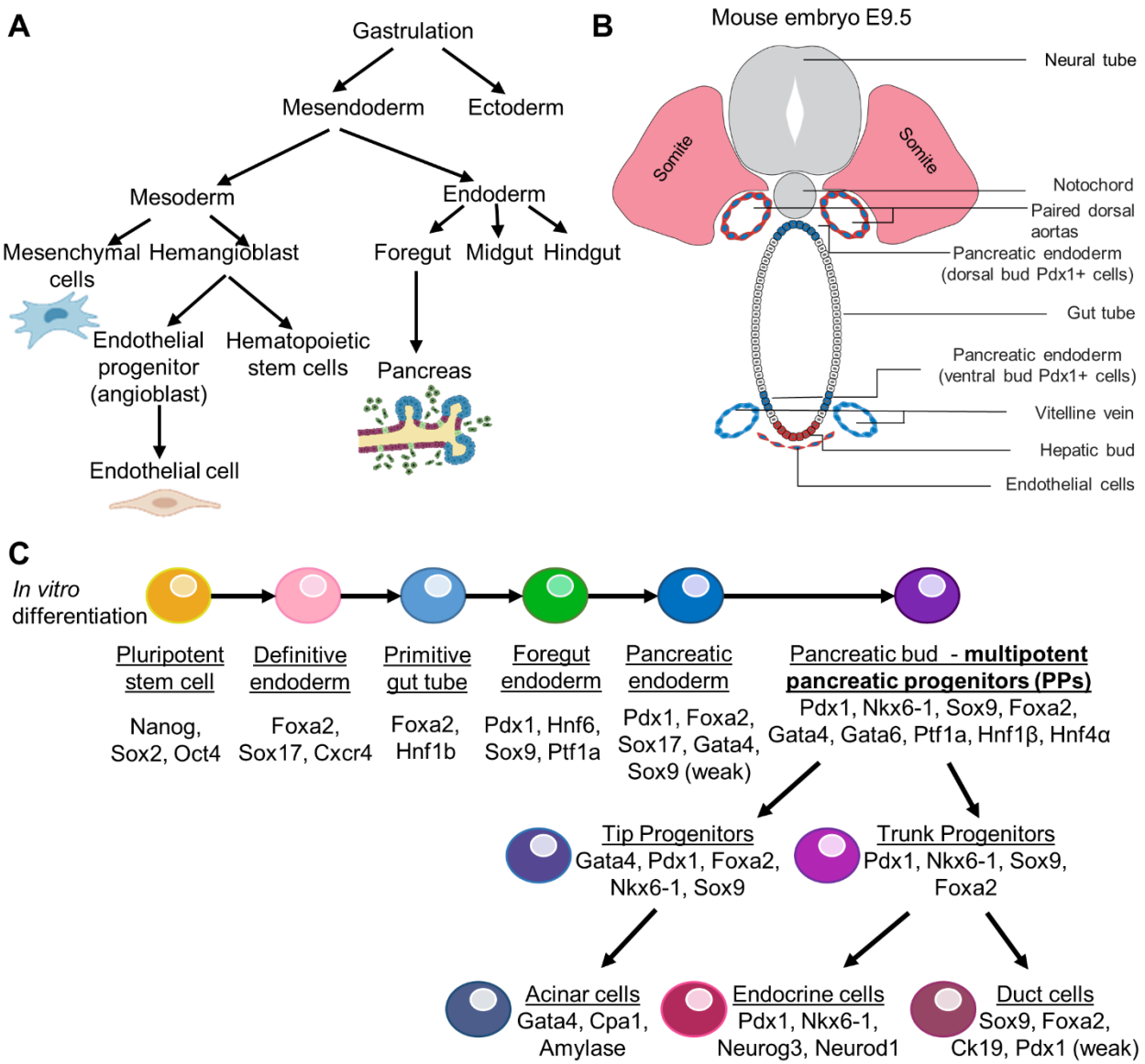

Figure S1. Pancreas development in the embryo and in vitro differentiation. A. Mouse embryo cell differentiation after gastrulation. The pancreas is derived from the foregut which is of endoderm origin. Endothelial and mesenchymal cells derive from the mesoderm germ layer. **B.** Cellular interactions in a E9.5 mouse embryo. On E9.5, pancreatic bud formation is induced by the signals secreted in proximal regions. Vascular endothelial growth factor (VEGF) is secreted by the neural tube and the foregut, and triggers dorsal aorta development. The dorsal aorta is composed only of endothelial cells that are in contact with the foregut endoderm. These endothelial cells instruct the formation of the pancreatic bud. This illustration is adopted with some modifications from (Ranjan et al., 2009). **C.** In vitro differentiation pipeline and marker genes in each state (Byrnes et al., 2018; Jennings et al., 2015; Prabakar et al., 2012; Shih et al., 2013).

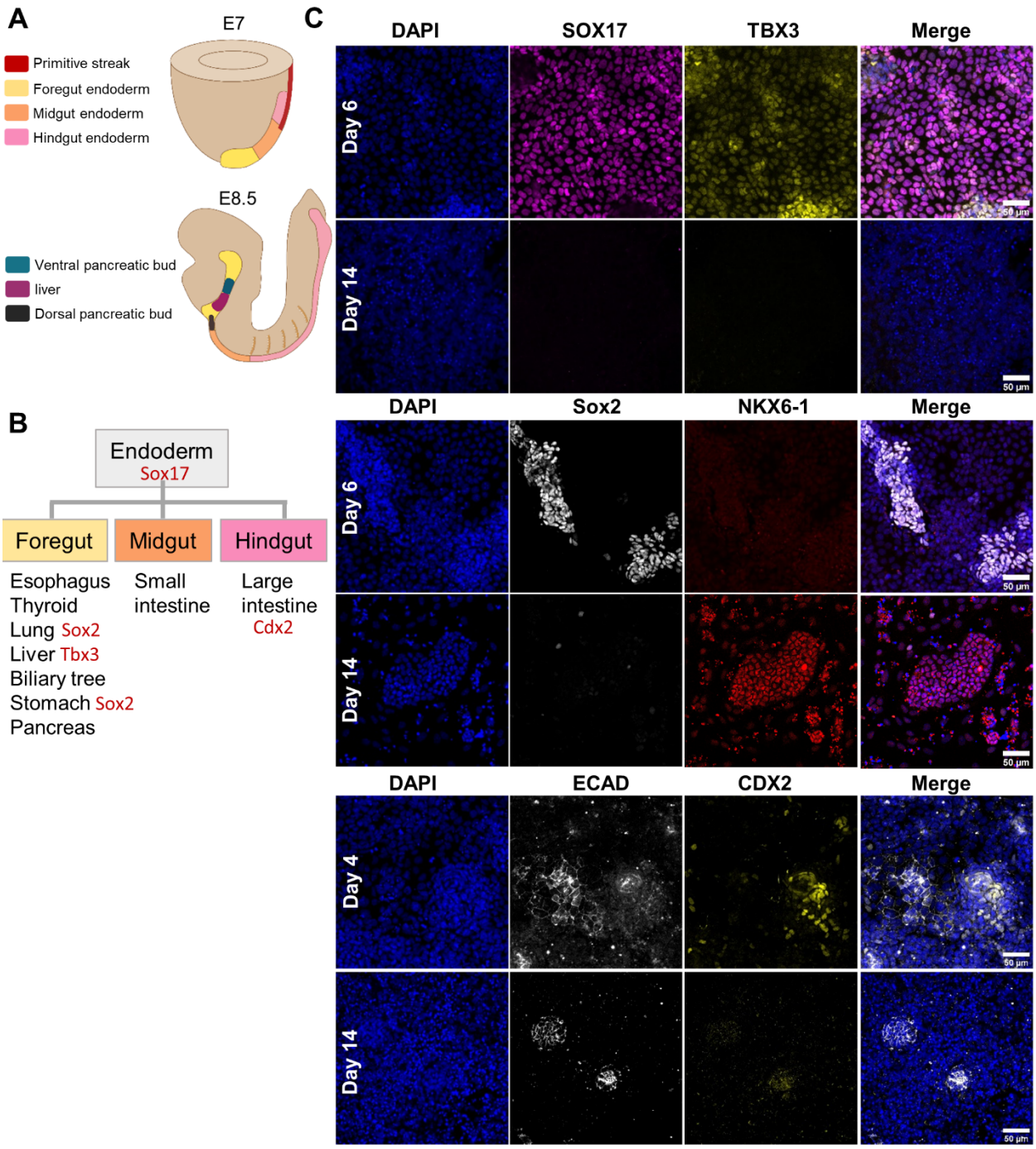

Figure S2. EpiSC differentiation to pancreatic progenitors is specific. A. Illustration of endoderm specification in the mouse embryo at E7 and E8.5. **B.** Endodermal organ development and marker genes. **C.** Confocal images along the course of EpiSC differentiation either on day 4 or day 6, reflecting the DE or GTE stages, respectively, and on day 14, i.e., the end of the differentiation. The cells were immunofluorescently stained for the markers listed in B, and for the pancreatic marker NKX6-1 and the epithelial marker ECAD. Note that at the end of differentiation, expression of the non-pancreatic endodermal markers diminished.

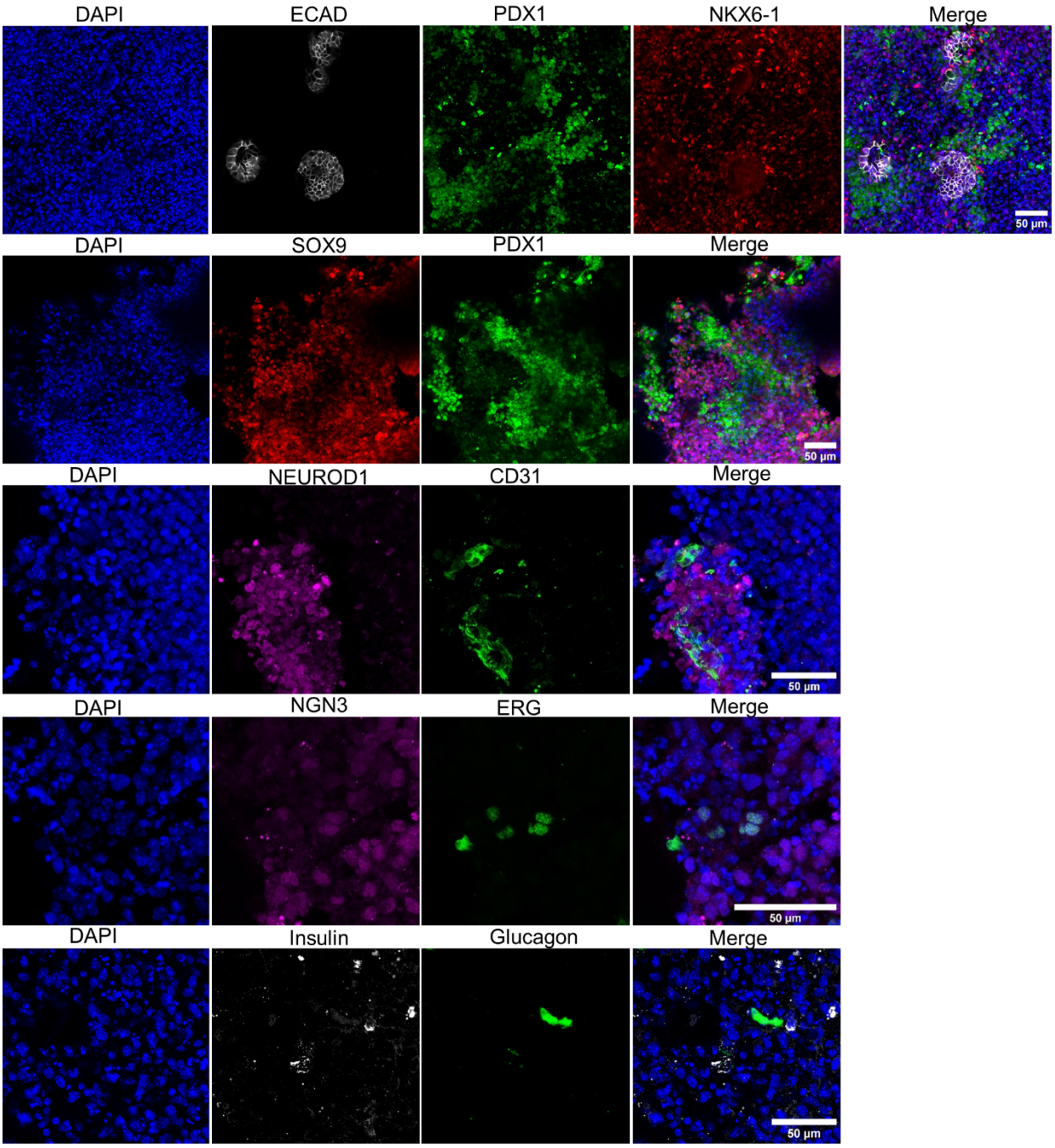

Figure S3. 3D aggregation of EpiSC-derived pancreas and mesoderm progenitors resulted in the expression of the various pancreas cell types. Confocal images of the organoids on day 8 after aggregation immunoflourescently stained for the progenitor markers NKX6-1, PDX1 and SOX9, endocrine markers NEUROD1 and NGN3 (Neurog3), endothelial markers ERG and CD31, an acinar marker AMY (Amylase), an epithelial marker ECAD, beta cell marker insulin and alpha cell marker glucagon.

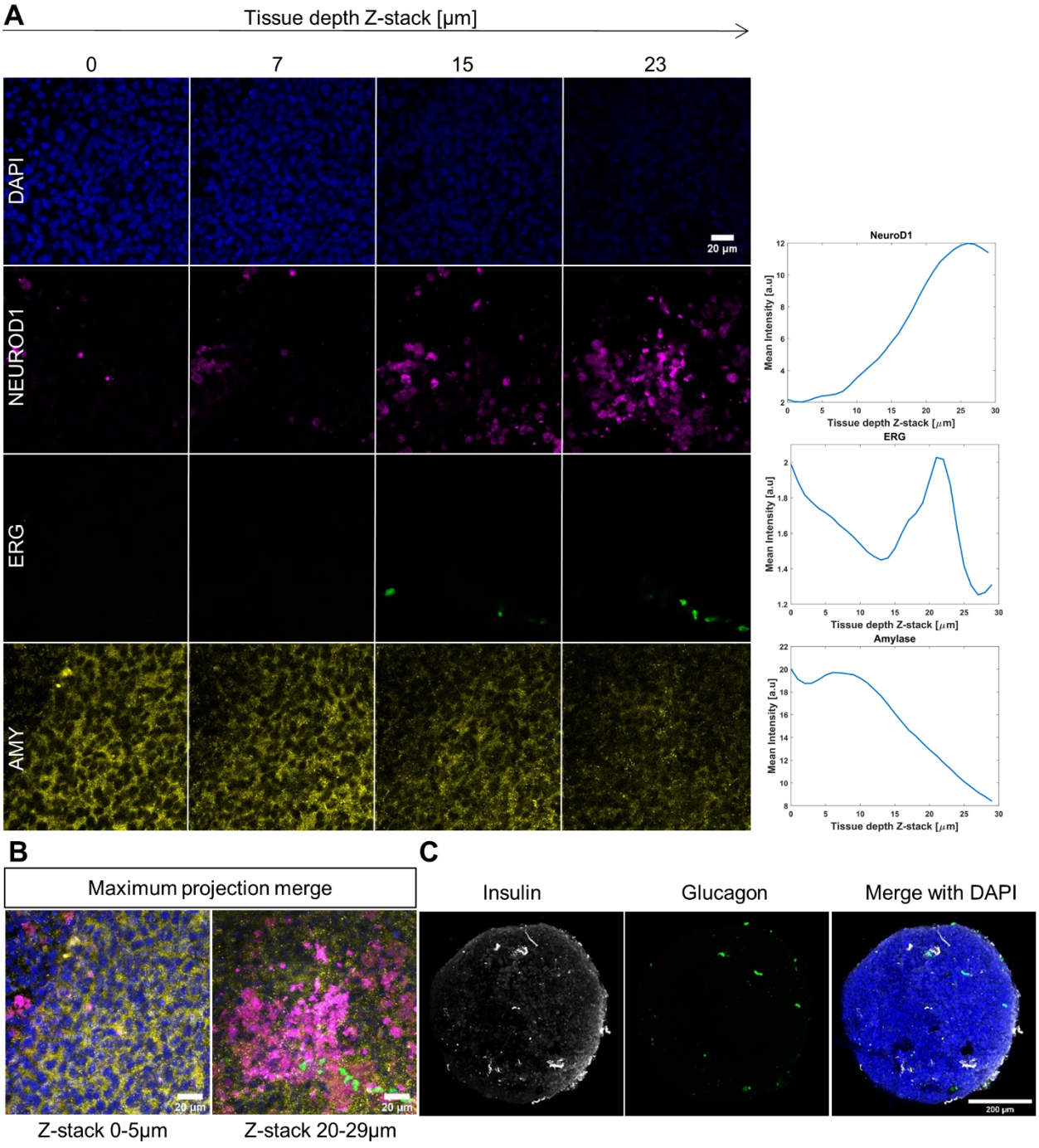

Figure S4. Endocrine cells are in proximity to endothelial cells. A. Left: confocal images of the organoids on day 8 after aggregation immunofluorescently stained for NEUROD1, ERG and AMY along the organoid depth (Z-stack). Right: The average intensity of each gene along the organoid depth. **B.** Maximum fluorescence intensity projection of the superficial Z-stacks (0-5µm) and inner Z-stacks (20-29µm) of the organoid confocal images as in A. **C.** Confocal images of a pancreatic organoid on day 8 AA immunofluorescently stained for glucagon and insulin, which mark alpha and beta cells, respectively. Nuclear staining with DAPI is in blue.

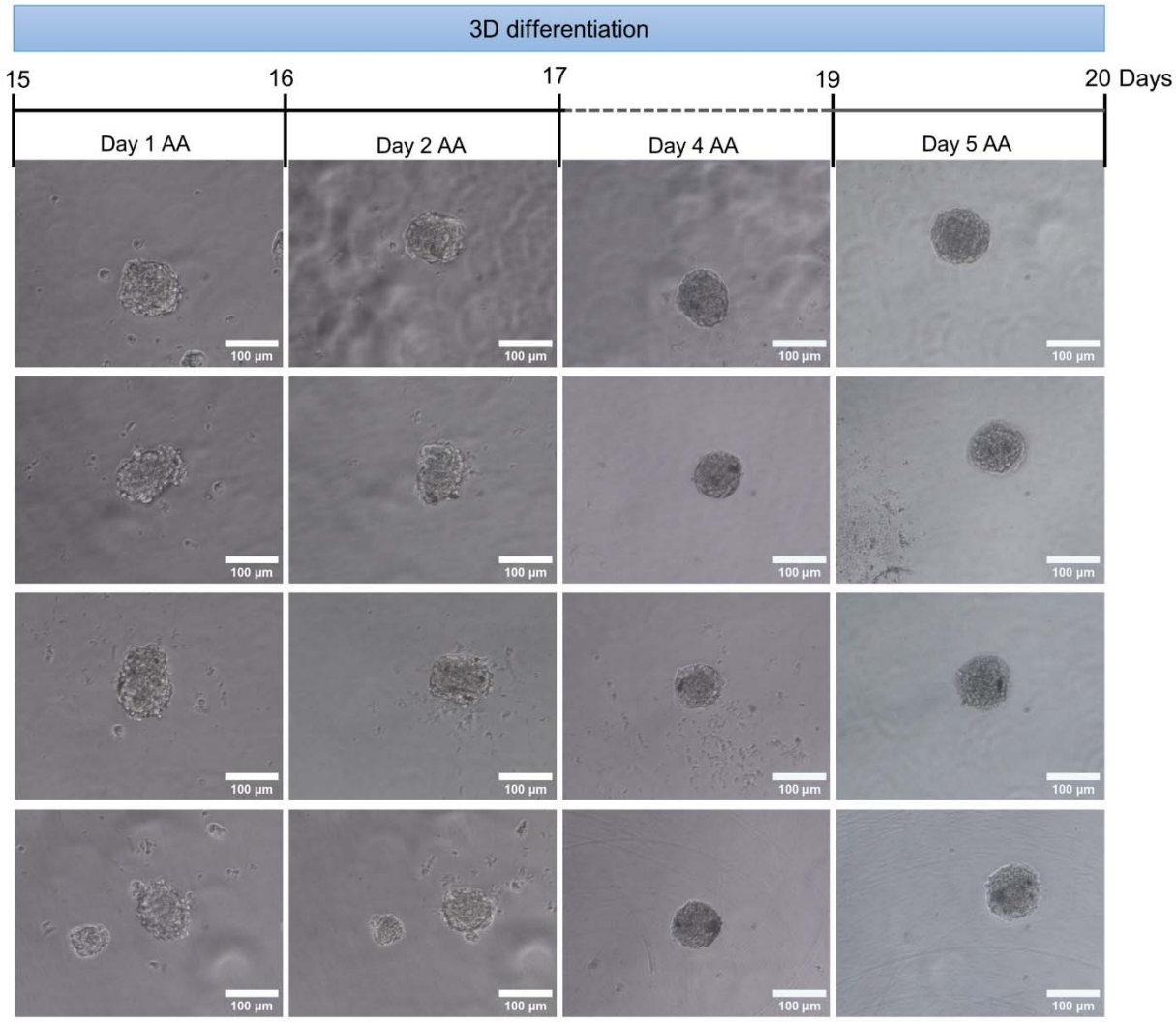

Figure S5. Aggregates do not grow without mesoderm progenitors. On day 14, 1000 PPs were plated in each well of a U-bottom 96-well plate. Brightfield images of the aggregates on days 1, 2, 4 and 5 after aggregation (AA). No change in the aggregate size was observed over time.

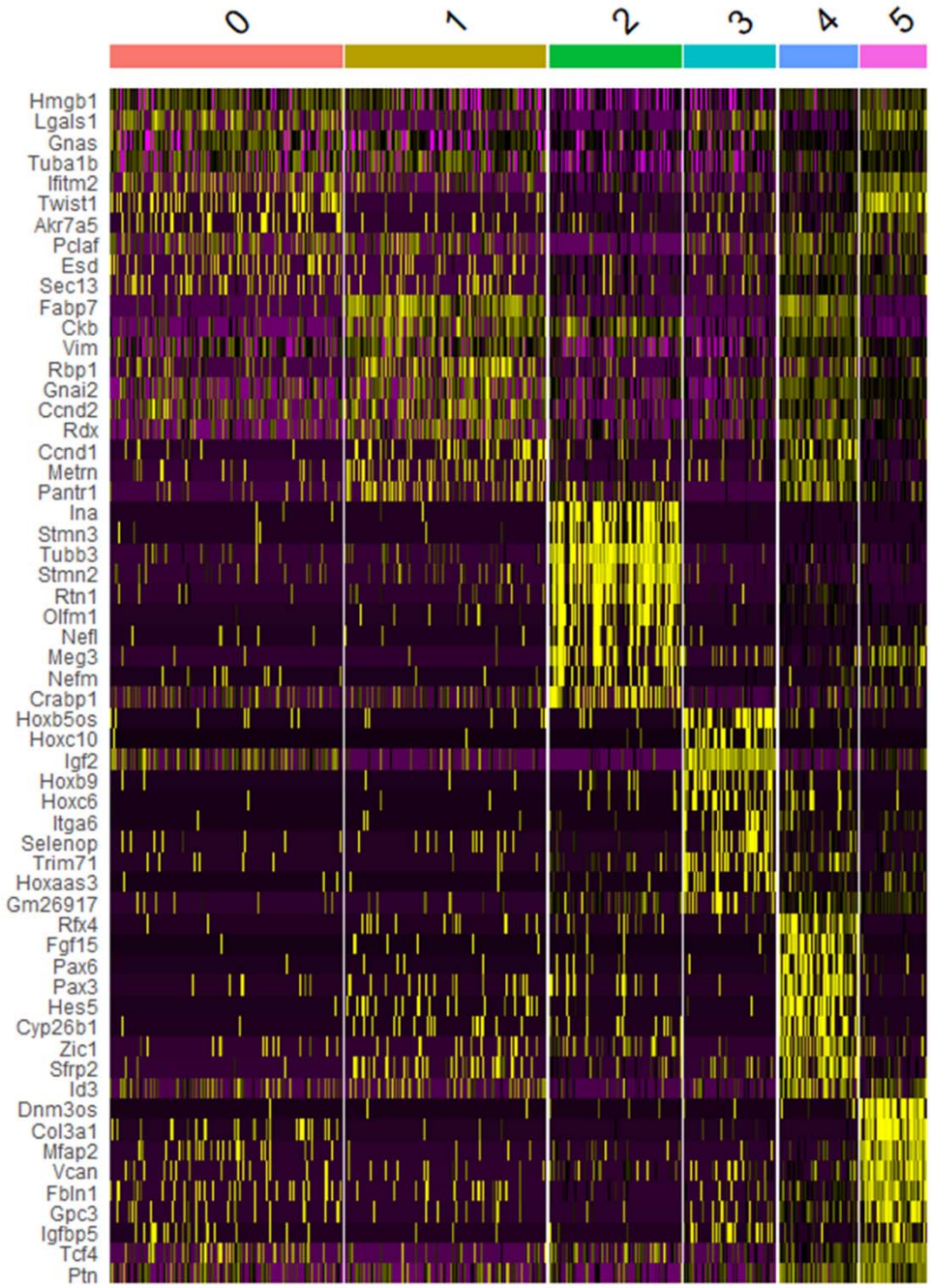

Figure S6. Gene markers of the organoid clusters. Expression heatmap of the top 10 gene markers for each cluster of the pancreatic organoid, as obtained using the Seurat R package (Hao et al., 2021).

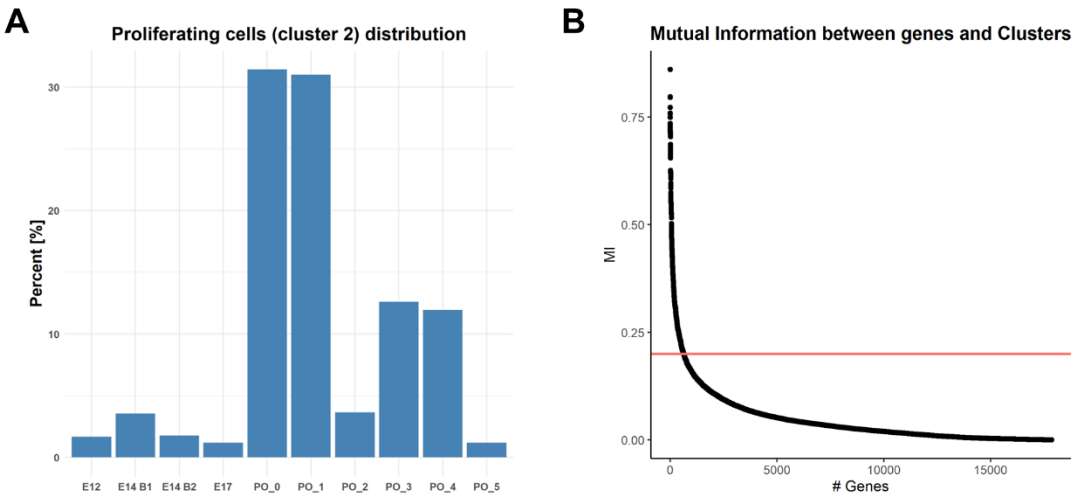

Figure S7. Selection of informative genes using mutual information. A. Sample composition of the proliferating cell cluster (cluster 2). PO_0 stands for pancreatic organoid cluster 0, PO_1 stands for pancreatic organoid cluster 1, and so forth. **B.** Mutual information (MI) calculation between expression of all the genes and cell assignment to the 5 clusters: progenitors, proliferating cells, erythroblast, myeloid, and acinar clusters. The horizontal red line indicates MI=0.2. Only genes with MI≥0.2 were used to calculate the cosine similarity (Fig. 7D) between the 6 organoid clusters in the proliferating cell group (A.) and the 4 known clusters.

Video S1. Movie showing confocal image Z-stacks of a total 70.15µm tissue depth of a pancreatic organoid embedded in 6.6% gelatin crosslinked with 5% microbial transglutaminase (mTG). CD31 (red) marks the vessel-like network and DAPI (blue) marks the nuclei.

References

Arda, H.E., Benitez, C.M., and Kim, S.K. (2013). Gene Regulatory Networks Governing Pancreas Development. Dev. Cell *25*, 5–13.

Azzarelli, R., Rulands, S., Nestorowa, S., Davies, J., Campinoti, S., Gillotin, S., Bonfanti, P., Göttgens, B., Huch, M., Simons, B., et al. (2018). Neurogenin3 phosphorylation controls reprogramming efficiency of pancreatic ductal organoids into endocrine cells. Sci. Rep. *8*.

Balak, J.R.A., Juksar, J., Carlotti, F., Lo Nigro, A., and de Koning, E.J.P. (2019). Organoids from the Human Fetal and Adult Pancreas. Curr. Diab. Rep. *19*.

Battiti, R. (1994). Using mutual information for selecting features in supervised neural net learning. IEEE Trans. Neural Networks *5*, 537–550.

Borowiak, M., Maehr, R., Chen, S., Chen, A.E., Tang, W., Fox, J.L., Schreiber, S.L., and Melton, D.A. (2009). Small Molecules Efficiently Direct Endodermal Differentiation of Mouse and Human Embryonic Stem Cells. Cell Stem Cell *4*, 348–358.

Byrnes, L.E., Wong, D.M., Subramaniam, M., Meyer, N.P., Gilchrist, C.L., Knox, S.M., Tward, A.D., Ye, C.J., and Sneddon, J.B. (2018). Lineage dynamics of murine pancreatic development at single-cell resolution. Nat. Commun. 2018 91 *9*, 1–17.

Chen, S., Borowiak, M., Fox, J.L., Maehr, R., Osafune, K., Davidow, L., Lam, K., Peng, L.F., Schreiber, S.L., Rubin, L.L., et al. (2009). A small molecule that directs differentiation of human ESCs into the pancreatic lineage. Nat. Chem. Biol. 2009 54 *5*, 258–265.

Delaspre, F., Massumi, M., Salido, M., Soria, B., Ravassard, P., Savatier, P., and Skoudy, A. (2013). Directed Pancreatic Acinar Differentiation of Mouse Embryonic Stem Cells via Embryonic Signalling Molecules and Exocrine Transcription Factors. PLoS One *8*, e54243.

Deschamps, J., and Duboule, D. (2017). Embryonic timing, axial stem cells, chromatin dynamics, and the Hox clock. Genes Dev. *31*, 1406–1416.

Edri, S., Hayward, P., Baillie-Johnson, P., Steventon, B., and Arias, A.M. (2019a). An Epiblast Stem Cell derived multipotent progenitor population for axial extension. Development dev.168187.

Edri, S., Hayward, P., Jawaid, W., and Martinez Arias, A. (2019b). Neuro-mesodermal progenitors (NMPs): a comparative study between pluripotent stem cells and embryo-derived populations. Development *146*, dev180190.

Fonseca, S.A.S., Costas, R.M., and Pereira, L.V. (2015). Searching for naïve human pluripotent stem cells. World J. Stem Cells *7*, 649.

Funata, M., Nio, Y., Erion, D.M., Thompson, W.L., and Takebe, T. (2020). The promise of human organoids in the digestive system. Cell Death Differ. 2020 281 *28*, 84–94.

Gao, S., Sun, Y., Zhang, X., Hu, L., Liu, Y., Chua, C.Y., Phillips, L.M., Ren, H., Fleming, J.B., Wang, H., et al. (2016). IGFBP2 activates the NF-κB pathway to drive epithelial-mesenchymal transition

and invasive character in pancreatic ductal adenocarcinoma. Cancer Res. *76*, 6543.

Georgia, S., investigation, A.B.-T.J. of clinical, and 2004, undefined β cell replication is the primary mechanism for maintaining postnatal β cell mass. Am Soc Clin Investig.

Ghezelayagh, Z., Zabihi, M., Kazemi Ashtiani, M., Ghezelayagh, Z., Lynn, F.C., and Tahamtani, Y. (2021). Recapitulating pancreatic cell–cell interactions through bioengineering approaches: the momentous role of non-epithelial cells for diabetes cell therapy. Cell. Mol. Life Sci. 2021 *1*, 1–26.

Glorieux, L., Sapala, A., Willnow, D., Moulis, M., Salowka, A., Darrigrand, J.F., Edri, S., Schonblum, A., Sakhneny, L., Schaumann, L., et al. (2022). Development of a 3D atlas of the embryonic pancreas for topological and quantitative analysis of heterologous cell interactions. Dev. *149*.

Gouzi, M., Kim, Y.H., Katsumoto, K., Johansson, K., and Grapin-Botton, A. (2011). Neurogenin3 initiates stepwise delamination of differentiating endocrine cells during pancreas development. Dev. Dyn. *240*, 589–604.

Grebenyuk, S., and Ranga, A. (2019). Engineering Organoid Vascularization. Front. Bioeng. Biotechnol. *7*.

Greggio, C., De Franceschi, F., Figueiredo-Larsen, M., Gobaa, S., Ranga, A., Semb, H., Lutolf, M., and Grapin-Botton, A. (2013). Artificial three-dimensional niches deconstruct pancreas development in vitro. Development *140*, 4452–4462.

Gupta, D., Santoso, J.W., and McCain, M.L. (2021). Characterization of Gelatin Hydrogels Cross-Linked with Microbial Transglutaminase as Engineered Skeletal Muscle Substrates. Bioeng. (Basel, Switzerland) *8*, 1–16.

Hao, Y., Hao, S., Andersen-Nissen, E., Mauck, W.M., Zheng, S., Butler, A., Lee, M.J., Wilk, A.J., Darby, C., Zager, M., et al. (2021). Integrated analysis of multimodal single-cell data. Cell *184*, 3573-3587.e29.

Hohwieler, M., Illing, A., Hermann, P.C., Mayer, T., Stockmann, M., Perkhofer, L., Eiseler, T., Antony, J.S., Müller, M., Renz, S., et al. (2017). Human pluripotent stem cell-derived acinar/ductal organoids generate human pancreas upon orthotopic transplantation and allow disease modelling. Gut *66*, 473–486.

Hori, Y., Fukumoto, M., and Kuroda, Y. (2008). Enrichment of Putative Pancreatic Progenitor Cells from Mice by Sorting for Prominin1 (CD133) and Platelet-Derived Growth Factor Receptor β. Stem Cells *26*, 2912–2920.

Huch, M., Bonfanti, P., Boj, S.F., Sato, T., Loomans, C.J.M., Van De Wetering, M., Sojoodi, M., Li, V.S.W., Schuijers, J., Gracanin, A., et al. (2013). Unlimited in vitro expansion of adult bi-potent pancreas progenitors through the Lgr5/R-spondin axis. EMBO J. *32*, 2708–2721.

Jennings, R.E., Berry, A.A., Strutt, J.P., Gerrard, D.T., and Hanley, N.A. (2015). Human pancreas development. Development *142*, 3126–3137.

Kim, S.Y., and Rane, S.G. (2011). The Cdk4-E2f1 pathway regulates early pancreas development by targeting Pdx1+ progenitors and Ngn3+ endocrine precursors. Development *138*, 1903–1912.

Kim, Y., Kim, H., Ko, U.H., Oh, Y., Lim, A., Sohn, J.W., Shin, J.H., Kim, H., and Han, Y.M. (2016). Islet-like organoids derived from human pluripotent stem cells efficiently function in the glucose responsiveness in vitro and in vivo. Sci. Rep. *6*.

Koike, H., Iwasawa, K., Ouchi, R., Maezawa, M., Giesbrecht, K., Saiki, N., Ferguson, A., Kimura, M., Thompson, W.L., Wells, J.M., et al. (2019). Modeling human hepato-biliary-pancreatic organogenesis from the foregut-midgut boundary. Nature *574*, 112.

Konstantinova, I., and Lammert, E. (2004). Microvascular development: learning from pancreatic islets. BioEssays *26*, 1069–1075.

Kuo, T.L., Cheng, K.H., Chen, L.T., and Hung, W.C. (2019). Deciphering The Potential Role of Hox Genes in Pancreatic Cancer. Cancers (Basel). *11*.

Kushner, J.A., Ciemerych, M.A., Sicinska, E., Wartschow, L.M., Teta, M., Long, S.Y., Sicinski, P., and White, M.F. (2005). Cyclins D2 and D1 Are Essential for Postnatal Pancreatic β-Cell Growth. Mol. Cell. Biol. *25*, 3752–3762.

Lammert, E., Cleaver, O., and Melton, D. (2001). Induction of pancreatic differentiation by signals from blood vessels. Science (80-.). *294*, 564–567.

Lammert, E., Cleaver, O., and Melton, D. (2003). Role of endothelial cells in early pancreas and liver development. Mech. Dev. *120*, 59–64.

Larsen, H.L., and Grapin-Botton, A. (2017). The molecular and morphogenetic basis of pancreas organogenesis. Semin. Cell Dev. Biol. *66*, 51–68.

Larsen, B.M., Hrycaj, S.M., Newman, M., Li, Y., and Wellik, D.M. (2015). Mesenchymal Hox6 function is required for mouse pancreatic endocrine cell differentiation. Dev. *142*, 3859–3868.

Lee, D.H., and Chung, H.M. (2011). Differentiation into Endoderm Lineage: Pancreatic differentiation from Embryonic Stem Cells. Int. J. Stem Cells *4*, 35.

Li, X.Y., Zhai, W.J., and Teng, C.B. (2016). Notch Signaling in Pancreatic Development. Int. J. Mol. Sci. *17*.

Liu, Z., Tanabe, K., Bernal-Mizrachi, E., and Permutt, M.A. (2008). Mice with beta cell overexpression of glycogen synthase kinase-3β have reduced beta cell mass and proliferation. Diabetologia *51*, 623–631.

Mamidi, A., Prawiro, C., Seymour, P.A., de Lichtenberg, K.H., Jackson, A., Serup, P., and Semb, H. (2018). Mechanosignalling via integrins directs fate decisions of pancreatic progenitors. Nature *564*, 114–118.

McCain, M.L., Agarwal, A., Nesmith, H.W., Nesmith, A.P., and Parker, K.K. (2014). Micromolded Gelatin Hydrogels for Extended Culture of Engineered Cardiac Tissues. Biomaterials *35*, 5462.

McCracken, K.W., and Wells, J.M. (2012). Molecular Pathways Controlling Pancreas induction. Semin. Cell Dev. Biol. *23*, 656.

Moreau, J.-F., Donaldson, D.D., Bennett, F., Witek-Giannotti, J., Clark, S.C., and Wong, G.G. (1988). Leukaemia inhibitory factor is identical to the myeloid growth factor human interleukin for DA cells. Nature *336*, 690–692.

Morgani, S., Nichols, J., and Hadjantonakis, A.-K. (2017). The many faces of Pluripotency: in vitro adaptations of a continuum of in vivo states. BMC Dev. Biol. *17*, 7.

Mulas, C., Kalkan, T., von Meyenn, F., Leitch, H.G., Nichols, J., and Smith, A. (2019). Defined conditions for propagation and manipulation of mouse embryonic stem cells. Development *146*, dev173146.

Nair, G.G., Liu, J.S., Russ, H.A., Tran, S., Saxton, M.S., Chen, R., Juang, C., Li, M. lan, Nguyen, V.Q., Giacometti, S., et al. (2019). Recapitulating endocrine cell clustering in culture promotes maturation of human stem-cell-derived β cells. Nat. Cell Biol. *21*, 263–274.

Nostro, M.C., Sarangi, F., Yang, C., Holland, A., Elefanty, A.G., Stanley, E.G., Greiner, D.L., and Keller, G. (2015). Efficient Generation of NKX6-1+ Pancreatic Progenitors from Multiple Human Pluripotent Stem Cell Lines. Stem Cell Reports *4*, 591–604.

Paguirigan, A.L., and Beebe, D.J. (2007). Protocol for the fabrication of enzymatically crosslinked gelatin microchannels for microfluidic cell culture. Nat. Protoc. 2007 27 *2*, 1782–1788.

Pan, F.C., and Wright, C. (2011). Pancreas organogenesis: From bud to plexus to gland. Dev. Dyn. *240*, 530–565.

Pierreux, C.E., Cordi, S., Hick, A.C., Achouri, Y., Ruiz de Almodovar, C., Prévot, P.P., Courtoy, P.J., Carmeliet, P., and Lemaigre, F.P. (2010). Epithelial: Endothelial cross-talk regulates exocrine differentiation in developing pancreas. Dev. Biol. *347*, 216–227.

Prabakar, K.R., Domínguez-Bendala, J., Damaris Molano, R., Pileggi, A., Villate, S., Ricordi, C., and Inverardi, L. (2012). Generation of Glucose-Responsive, Insulin-Producing Cells from Human Umbilical Cord Blood-Derived Mesenchymal Stem Cells. Cell Transplant. *21*, 1321–1339.

Quilichini, E., and Haumaitre, C. (2015). Implication of epigenetics in pancreas development and disease. Best Pract. Res. Clin. Endocrinol. Metab. *29*, 883–898.

Ranjan, A.K., Joglekar, M. V, and Hardikar, A. (2009). Endothelial cells in pancreatic islet development and function.

Rossi, G., Manfrin, A., and Lutolf, M.P. (2018). Progress and potential in organoid research. Nat. Rev. Genet. *19*, 671–687.

Rukstalis, J.M., and Habener, J.F. (2007). Snail2, a mediator of epithelial-mesenchymal transitions, expressed in progenitor cells of the developing endocrine pancreas. Gene Expr. Patterns *7*, 471–479.

Scavuzzo, M.A., Hill, M.C., Chmielowiec, J., Yang, D., Teaw, J., Sheng, K., Kong, Y., Bettini, M.,

Zong, C., Martin, J.F., et al. (2018). Endocrine lineage biases arise in temporally distinct endocrine progenitors during pancreatic morphogenesis. Nat. Commun. 2018 91 *9*, 1–21.

Schaffer, A.E., Freude, K.K., Nelson, S.B., and Sander, M. (2010). Nkx6 Transcription Factors and Ptf1a Function as Antagonistic Lineage Determinants in Multipotent Pancreatic Progenitors. Dev. Cell *18*, 1022–1029.

Seymour, P.A., and Serup, P. (2019). Mesodermal induction of pancreatic fate commitment. Semin. Cell Dev. Biol. *92*, 77–88.

Sharon, N., Chawla, R., Mueller, J., Vanderhooft, J., Whitehorn, L.J., Rosenthal, B., Gürtler, M., Estanboulieh, R.R., Shvartsman, D., Gifford, D.K., et al. (2019a). A Peninsular Structure Coordinates Asynchronous Differentiation with Morphogenesis to Generate Pancreatic Islets. Cell *176*, 790-804.e13.

Sharon, N., Vanderhooft, J., Straubhaar, J., Mueller, J., Chawla, R., Zhou, Q., Engquist, E.N., Trapnell, C., Gifford, D.K., and Melton, D.A. (2019b). Wnt Signaling Separates the Progenitor and Endocrine Compartments during Pancreas Development. Cell Rep. *27*.

Shih, H.P., Wang, A., and Sander, M. (2013). Pancreas Organogenesis: From Lineage Determination to Morphogenesis. Http://Dx.Doi.Org/10.1146/Annurev-Cellbio-101512-122405 *29*, 81–105.

Smith, A.G., Heath, J.K., Donaldson, D.D., Wong, G.G., Moreau, J., Stahl, M., and Rogers, D. (1988). Inhibition of pluripotential embryonic stem cell differentiation by purified polypeptides. Nature *336*, 688–690.

Sneddon, J.B., Borowiak, M., and Melton, D.A. (2012). Self-renewal of embryonic-stem-cell-derived progenitors by organ-matched mesenchyme. Nature *491*, 765–768.

Talavera-Adame, D. (2015). Endothelium-derived essential signals involved in pancreas organogenesis. World J. Exp. Med. *5*, 40.

Tam, P.P.., and Behringer, R.R. (1997). Mouse gastrulation: the formation of a mammalian body plan. Mech. Dev. *68*, 3–25.

Tosolini, M., and Jouneau, A. (2015). From Naive to Primed Pluripotency: In Vitro Conversion of Mouse Embryonic Stem Cells in Epiblast Stem Cells. (Humana Press, New York, NY), pp. 209–216.

Tsuchiya, B., Sato, Y., Kameya, T., Okayasu, I., and Mukai, K. (2006). Differential expression of N-cadherin and E-cadherin in normal human tissues. Arch. Histol. Cytol. *69*, 135–145.

Vanitha, C.D.A., Devaraj, D., and Venkatesulu, M. (2015). Gene Expression Data Classification Using Support Vector Machine and Mutual Information-based Gene Selection. Procedia Comput. Sci. *47*, 13–21.

Villasenor, A., Chong, D.C., Henkemeyer, M., and Cleaver, O. (2010). Epithelial dynamics of pancreatic branching morphogenesis. Development *137*, 4295–4305.

Williams, R.L., Hilton, D.J., Pease, S., Willson, T.A., Stewart, C.L., Gearing, D.P., Wagner, E.F., Metcalf, D., Nicola, N.A., and Gough, N.M. (1988). Myeloid leukaemia inhibitory factor maintains the developmental potential of embryonic stem cells. Nature *336*, 684–687.

Wray, J., Kalkan, T., and Smith, A.G. (2010). The ground state of pluripotency. Biochem. Soc. Trans. *38*, 1027–1032.

Wu, Y., Aegerter, P., Nipper, M., Ramjit, L., Liu, J., and Wang, P. (2021). Hippo Signaling Pathway in Pancreas Development. Front. Cell Dev. Biol. *9*, 1132.

Ying, Q.-L., Wray, J., Nichols, J., Batlle-Morera, L., Doble, B., Woodgett, J., Cohen, P., and Smith, A. (2008). The ground state of embryonic stem cell self-renewal. Nature *453*, 519–523.

Young, T., Rowland, J.E., van de Ven, C., Bialecka, M., Novoa, A., Carapuco, M., van Nes, J., de Graaff, W., Duluc, I., Freund, J.-N., et al. (2009). Cdx and Hox genes differentially regulate posterior axial growth in mammalian embryos. Dev. Cell *17*, 516–526.

Yung, C.W., Wu, L.Q., Tullman, J.A., Payne, G.F., Bentley, W.E., and Barbari, T.A. (2007). Transglutaminase crosslinked gelatin as a tissue engineering scaffold. J. Biomed. Mater. Res. Part A *83A*, 1039–1046.